AFRL-RQ-WP-TP-2023-0006

TWO-DIMENSIONAL TRANSITIONAL MACH 6 FLOW AND A FRAMEWORK FOR UPSTREAM INFLUENCE

James H. Miller
Aerospace Systems Directorate

MARCH 2024
Interim Report

AIR FORCE RESEARCH LABORATORY
AEROSPACE SYSTEMS DIRECTORATE
WRIGHT-PATTERSON AIR FORCE BASE, OH 45433-7542
AIR FORCE MATERIEL COMMAND
UNITED STATES AIR FORCE

NOTICE PAGE

AFRL-RQ-WP-TP-2023-0006 has been reviewed and is approved for publication in accordance with assigned distribution statement.

REPORT DOCUMENTATION PAGE

PLEASE DO NOT RETURN YOUR FORM TO THE ABOVE ORGANIZATION.

1. REPORT DATE	2. REPORT TYPE	3. DATES COVERED	
		START DATE	END DATE
08032024	Interim	01012020	10012022

4. TITLE AND SUBTITLE

TWO-DIMENSIONAL TRANSITIONAL MACH 6 FLOW AND A FRAMEWORK FOR UPSTREAM INFLUENCE

5a. CONTRACT NUMBER	5b. GRANT NUMBER	5c. PROGRAM ELEMENT NUMBER
		62201F
5d. PROJECT NUMBER	**5e. TASK NUMBER**	**5f. WORK UNIT NUMBER**
		Q1K7

6. AUTHOR(S)

James H. Miller

7. PERFORMING ORGANIZATION NAME(S) AND ADDRESS(ES)

Aerospace Systems Directorate
Air Force Research Laboratory
Air Force Materiel Command
Wright-Patterson Air Force Base, OH 45433-7542

8. PERFORMING ORGANIZATION REPORT NUMBER

9. SPONSORING/MONITORING AGENCY NAME(S) AND ADDRESS(ES)	10. SPONSOR/MONITOR'S ACRONYM(S)	11. SPONSOR/MONITOR'S REPORT NUMBER(S)
Aerospace Systems Directorate Air Force Research Laboratory Air Force Materiel Command Wright-Patterson Air Force Base, OH 45433-7542	AFRL/RQHA	AFRL-RQ-WP-TP-2023-0006

12. DISTRIBUTION/AVAILABILITY STATEMENT

DISTRIBUTION STATEMENT A. Approved for public release. Distribution is unlimited; May 2022

13. SUPPLEMENTARY NOTE

PA Clearance Number: AFRL-2022-4773; Clearance Date: Oct. 5, 2022.

14. ABSTRACT

Two sets of experimental results are presented in this paper. One set is for a flat plate configuration that is used to characterize the transitional flow in the absence of a 16 degree compression ramp. The second set of results is for the compression ramp itself. The freestream Mach number of the flow is 5.85, with a freestream Reynolds number ranging from 10x10^6 to 30x10^6 per foot. In addition, the scaling of upstream influence is discussed and compared to other scaling studies for laminar, transitional, and turbulent flows. It is believed that the present framework can be used to characterize upstream influence for a wide range of flows.

15. SUBJECT TERMS

Upstream Influence, Similarity Laws, Compression Ramp, Boundary Layer Transition

16. SECURITY CLASSIFICATION OF:			17. LIMITATION OF ABSTRACT	18. NUMBER OF PAGES
a. REPORT	b. ABSTRACT	C. THIS PAGE		
Unclassified	Unclassified	Unclassified	SAR	40

19a. NAME OF RESPONSIBLE PERSON	19b. PHONE NUMBER *(Include area code)*
JAMES H. MILLER	(937) 255-7212

PREVIOUS EDITION IS OBSOLETE.

STANDARD FORM 298 (REV. 5/2020)
Prescribed by ANSI Std. Z39.18

Two-Dimensional Transitional Mach 6 Flow and a Framework for Upstream Influence

James H. Miller[1]
Air Force Research Laboratory, Hypersonic Sciences Branch, High Speed Systems Division, Wright-Patterson Air Force Base, Ohio, 45433, USA

Two sets of experimental results are presented in this paper. One set is for a flat plate configuration that is used to characterize the transitional flow in the absence of a 16 degree compression ramp. The second set of results is for the compression ramp itself. The freestream Mach number of the flow is 5.85, with a freestream Reynolds number ranging from 10x10^6 to 30x10^6 per foot. The experimental results include two conditions for the wall temperature: a cold wall condition and an adiabatic wall condition. Pressure measurements were taken to sufficiently describe the upstream influence of the compression ramp. Laminar and turbulent RANS CFD results are compared to experimental data. Downstream influence was not able to be determined from the experimental data at the time of this writing. Scaling of the influence lengths driven by the inviscid pressure jump at the ramp plate juncture are discussed for upstream influence. In addition, the scaling of upstream influence is discussed and compared to other scaling studies for laminar, transitional, and turbulent flows. It is believed that the present framework can be used to characterize upstream influence for a wide range of flows.

I. Nomenclature

C_{f0} = Skin friction coefficient at the beginning of the interaction (Roshko & Thomke notation)
C_{f0}^* = Skin friction coefficient intercept (Roshko & Thomke notation)
C_p = pressure coefficient, $C_p = \frac{p-p_\infty}{1/2\,\rho_\infty V_\infty^2}$
C_w = Chapman-Rubesin constant
l = length of elliptic region, *m*
L = reference length, *m*
L^* = upstream influence length (Sourverein et al. notation)
$\frac{l_u}{\delta_L}$ = ratio of upstream influence length to undisturbed (flat plate) boundary layer thickness
$\frac{l}{\delta_L}$ = ratio of elliptic region length to undisturbed (flat plate) boundary layer thickness
l_u = length of upstream influence length, *m*
l_d = length of downstream influence length, *m*
M = Mach number, ratio of velocity to speed of sound, $M = \frac{V}{\sqrt{\gamma\, p/\rho}}$
p = pressure, N/m^2
Re = Reynolds number, ratio of inertia forces to viscous forces, $Re = \frac{\rho_\infty V_\infty L}{\mu_\infty}$
Re_δ = Reynolds number based on boundary layer thickness
Re_θ = Reynolds number based on momentum thickness
Re_x = Reynolds number based on local x station

[1] Principal Aerospace Engineer, Hypersonic Sciences Branch, AIAA Associate Fellow.
Distribution Statement A: Approved for public release; Distribution is unlimited. PA# AFRL-2022-4773; Cleared 10/05/2022.

Distribution Statement A: Approved for public release; Distribution is unlimited. PA# AFRL-2022-4773; Cleared 10/05/2022.

$Re\frac{C_p}{2}$ = Ratio of pressure forces to viscous forces–(interaction parameter for upstream & downstream influence)
$Re_\delta\frac{C_p}{2}$= Ratio of pressure forces to viscous forces – (shape factor in incompressible boundary layer theory)
S_e^* = Separation strength parameter (Souverein et al. notation)
T = static temperature
u,v,w = Cartesian velocity components in the x,y,z directions respectively, *m/s*
V_∞ = reference or freestream velocity, *m/s*
x,y,z = Cartesian coordinates, *m*
Δp = reference change in pressure relative to freestream (e.g., p_c - p_∞, where p_c is the inviscid pressure downstream of a shock interaction with a flat surface or compression ramp), N/m^2
δ = boundary layer thickness at location x
δ_L = boundary layer thickness at location L, *m*
δ_0 = boundary layer thickness for undisturbed conditions at corner location in absence of interaction (Settles et al. notation)
δ_{in}^* = displacement thickness incoming to shock boundary layer interaction (Souverein et al. notation)
β = shock angle generated by compression ramp, degrees (Souverein et al. notation)
φ = compression ramp angle, degrees (Souverein et al. notation)
k = viscous component of Souverein et al. scaling
γ = ratio of specific heats, 1.4 for air.
θ, α = compression ramp angle, degrees
τ = shear stress, N/m^2
μ = viscosity, *kg / (m s)*

Superscripts:

~ = nondimensional quantity normalized by freestream conditions or reference change in pressure

Subscripts:

aw = adiabatic wall
d = downstream boundary of elliptic region
L = x location of compression ramp leading edge or shock impingement point
u = upstream boundary of elliptic region
x = x location
xx,xy = Cartesian components of shear stress
∞ = freestream conditions

II. Introduction

The characterization of upstream influence in shock boundary layer interactions (SBLIs) has been a topic of interest since the late 1930s [1]. Understanding this phenomenon can help to maximize the useful data extracted from measurement efforts and help aid configuration designers in placement of key geometry components such as control surfaces, canards, or wings. Understanding upstream and downstream influence can also help improve productivity of computational analysis by enabling greater computational resources to be used only where needed [2]. Further, this understanding can improve approaches to reduce uncertainty in control authority for hypersonic vehicles.

The focus on the problem of upstream influence has been on supersonic viscous flows for many decades, and that is the focus of the present paper. However, the new framework presented in the present paper is believed to be extensible to subsonic and incompressible flows, as discussed by Lighthill [3] and Chapman et al [4]. For the problem of upstream influence caused by a SBLI, there are several papers with excellent reviews that can provide helpful context [5-7]. Additional mathematical treatment of the problem is discussed by Lighthill [8,9].

The original motivation of the present work was to document some recent experimental results for a high Reynolds number, transitional flow at Mach 6 over flat plate and compression ramp geometries. As the research unfolded, it became clear that a discussion of transitional upstream influence should include observations from the laminar and turbulent research documented in the literature to provide appropriate context. Additionally, the author has realized that many different aspects of the upstream influence problem are of interest to the technical community. Predictions and correlations for plateau pressure, incipient separation angle, peak heating, and frequency of shock oscillation are some examples where progress has been made in understanding. While these are important studies, the present paper is not focused on these topic areas. In addition to documenting some recent experimental results, the present paper addresses a more applied question – such as what range of values should be expected for upstream influence for 2D supersonic flow over a compression ramp in laminar, transitional, and turbulent flows? And to limit the scope further,

we consider adiabatic wall conditions. It is fortunate that today there are sufficient data to develop a useful framework to characterize previous correlations and provide a baseline for future efforts to expand to other flow conditions and geometries.

The starting point for research efforts in high Mach number transitional flows over compression ramps begins with the work of Chapman et al. [4] where there was an extensive study on flow separation in SBLIs including the effects of transition involving steps, bases, compression corners, and curved surfaces. Needham and Stollery [10] focused on boundary layer separation and found that boundary layer transition can significantly affect the pressure coefficient required for incipient separation. Roberts [11] found that the length of the transitional flow separation depended on the freestream Mach number, inviscid pressure rise at the compression corner and the length over which transition develops in an attached flow, flat-plate boundary layer with the same external flow conditions. Gray and Rhudy [12] investigated the effects of nose radius on the flat plate and the effects of cooling in separation over a compression ramp at Mach numbers from 3 to 6. Holden and Chadwick [13] found that the running length of the transitional region of the flow is significantly shortened when in the presence of an adverse pressure gradient. Knight and Mortazavi recently reviewed transitional SBLIs in the hypersonic range [14].

A computational approach to the flow stability problem was performed by Balakumar et al. [15] in 2002 who concluded that the boundary layer transition will only happen downstream of the separated region due to the second mode instability for the conditions considered. Whalen et al. [16] investigated transitional and turbulent flows at Mach 6 over a compression corner and found that convection of second-mode-like waves into the SWBLI produced a wave/shocklet doublet over a wide range of ramp angles. Threadgill et al. [17] found that downstream features of a transitional SBLI lead the motion of the separation shock and that disturbances propagate upstream before inducing motion of the separation shock. They conclude that transitional SBLIs can provide a means to isolate and investigate downstream mechanisms that drive the low-frequency shock motion. Cao et al. [18] applied DNS to a Mach 7.7 flow over a compression ramp and found that the transition of the boundary layer is initiated by its intrinsic instability and progresses through a breakdown of streamwise vortices. All of these studies provide key insight into compression ramp flows in which there is boundary layer transition. One of the aims of the present paper is to share insight and results from recent testing of a transitional flow over a flat plate and flow over a flat plate / compression ramp geometry. Following the presentation of the experimental results, the paper will focus on the characterization of upstream influence data in a new framework for laminar, transitional and turbulent flows.

III. Experimental Facility and Setup

The Mach 6 High Reynolds Number Facility is an intermittent, blow-down hypersonic wind tunnel with an axisymmetric 12 inch exit diameter nozzle that produces a uniform Mach 6 flow in an open jet test section. The open jet has a core flow diameter of 10 inches in diameter. The Reynolds number can range from 10 to 30 million / ft. The stagnation temperature can range from 900 R to 1100 R (Ref. [19]). The facility was returned to operation in 2014 and has included programs with measurements of heat transfer, boundary layer transition, configuration performance/stability/control and advanced diagnostic methods. The models used in the testing campaigns are shown in Fig. 2.

Figure 1 Mach 6 High Reynolds Number Facility.

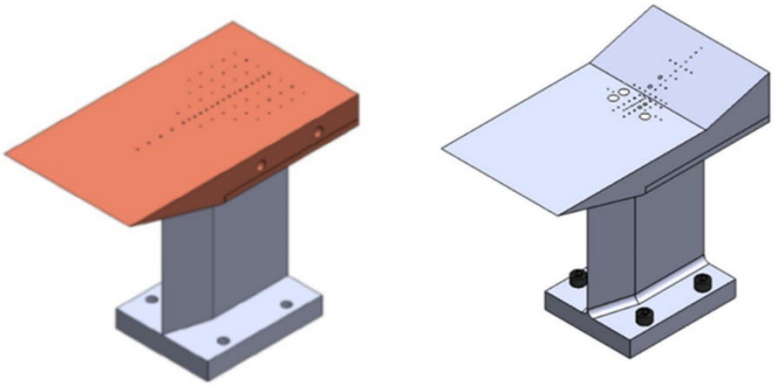

Figure 2 Flat plate (copper) and compression ramp (stainless steel) mounted on wind tunnel strut.

IV. Experimental Results

A. Flat Plate

The flat plate geometry was run for cold wall and adiabatic wall conditions. The flat plate model is 10 inches long and 6 inches wide. The compression ramp model has a flat plate section that is 7 inches long and a ramp section that is 3 inches long. The compression ramp angle is 16 degrees.. Some results for the compression ramp have been reported in a previous paper [20]. The maximum surface roughness for each polished model was measured to be less than 16 microinches. For the highest Reynolds number condition of about 30 million per foot, this equates to a roughness Reynolds number of about 40. This was deemed appropriate to avoid early boundary layer transition due to roughness on the surface Ref. [21,22]. The stagnation temperature for all of the experimental runs in this paper was 900 R. The freestream Mach number was 5.85, based on previous calibration studies and more recent freestream characterization [23].

The first series of testing was on the flat plate model and sample results for cold wall flows are in Figs. 3 and 4.

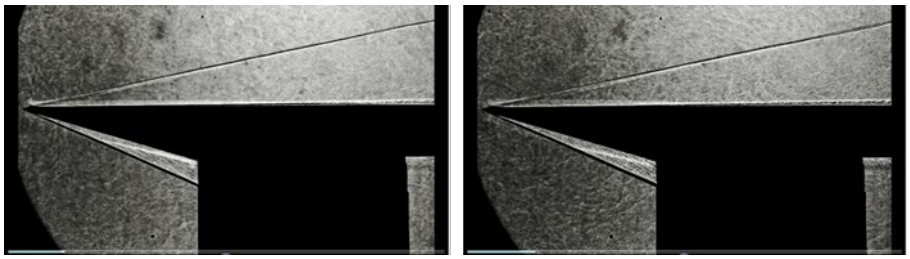

Figure 3 Shadowgraph results for Po = 700 (left) and 1000 psi (right). Note the presence of acoustic waves after the flow transitions to turbulent.

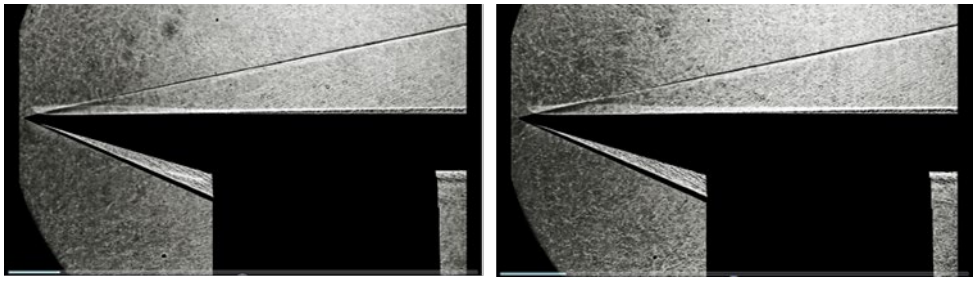

Figure 4 Shadowgraph results for Po = 1400 (left) and 2000 psi (right). Note the presence of acoustic waves are stronger and appear closer to the leading edge of the plate as Po increases (increasing Reynolds number).

The broadband acoustic waves coming from the flat plate boundary layer are more pronounced as the Reynolds number is increased through an increase in the stagnation pressure of the test. The heat transfer results are shown in Figs. 5 and 6 where the Stanton number and Reynolds number have been rewritten in terms of the incompressible variables of Spalding and Chi [24-26].

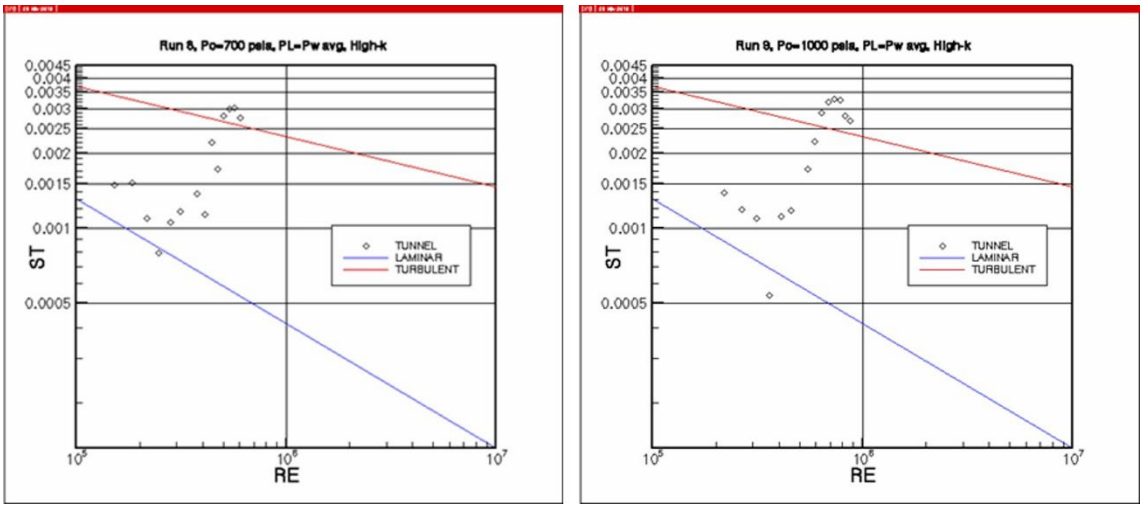

Figure 5 Heat transfer results compared to laminar and turbulence theory for Po = 700 psi (left) and Po = 1000 psi (right).

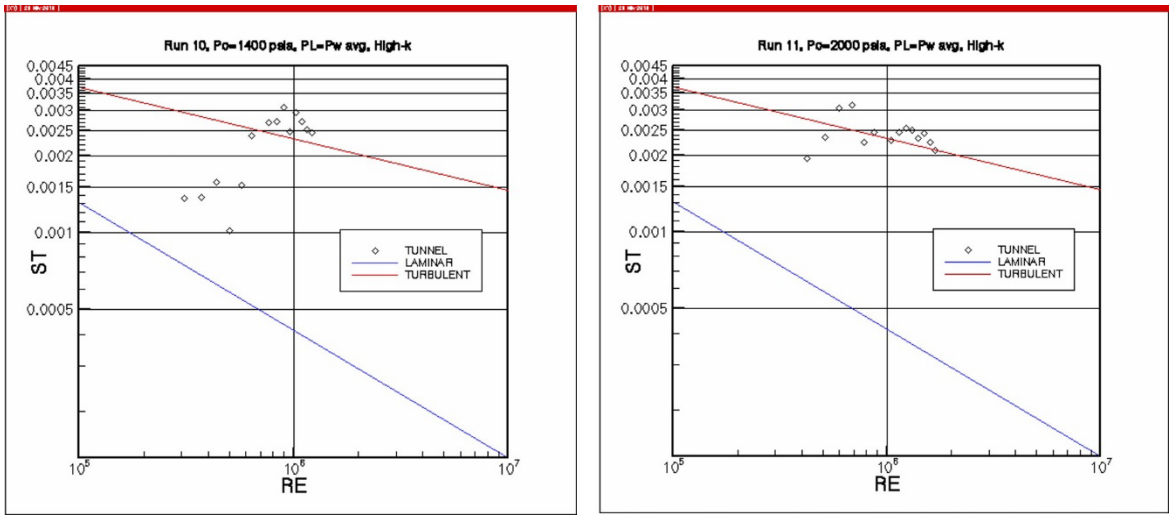

Figure 6 Heat transfer results compared to laminar and turbulent theory for Po = 1400 psi (left) and Po = 2000 psi (right).

The location of the start of boundary layer transition for the present experiments was determined from the heat transfer results in Figs. 5 and 6. Comparison is made to previous flat plate results obtained from the same test facility [19] in Fig. 7– showing that the present results are consistent with the results from the same facility around 1994.

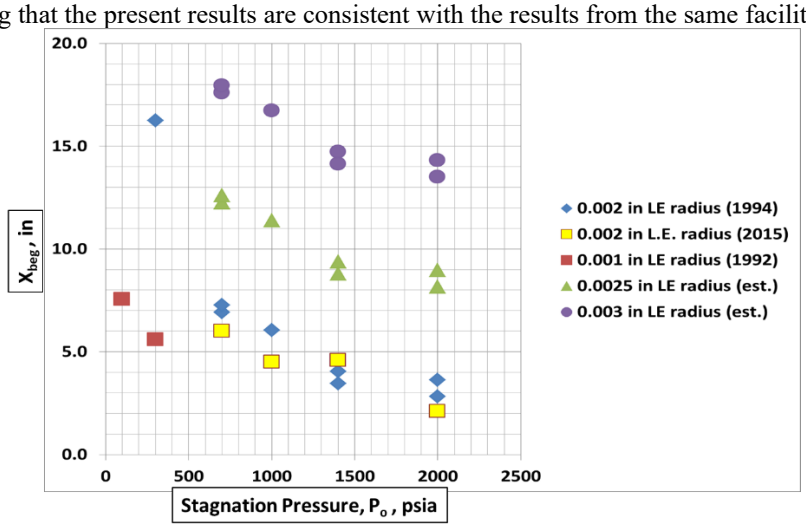

Figure 7 Comparison of boundary layer transition location vs. Po for several nose radii. Present results are consistent with previous results obtained from same facility in 1992. Estimates using theory are included for larger nose radii (0.0025 and 0.003 in).

The results of two-color schlieren [27] are shown in Fig. 8 with the measurement line taken at 7 inches downstream of the leading edge. In Fig. 9, the boundary layer thickness at several axial stations is derived from the peak intensity level location of the color Schlieren. The thickness obtained from this approach is consistent with boundary layer measurements for flat plates at these tunnel conditions. Results from early CFD analysis for the flat plate are shown in Figs. 10 and 11. The CFD demonstrates that the high gradient region of the density is a close approximation to the edge of the boundary layer determined from velocity profiles.

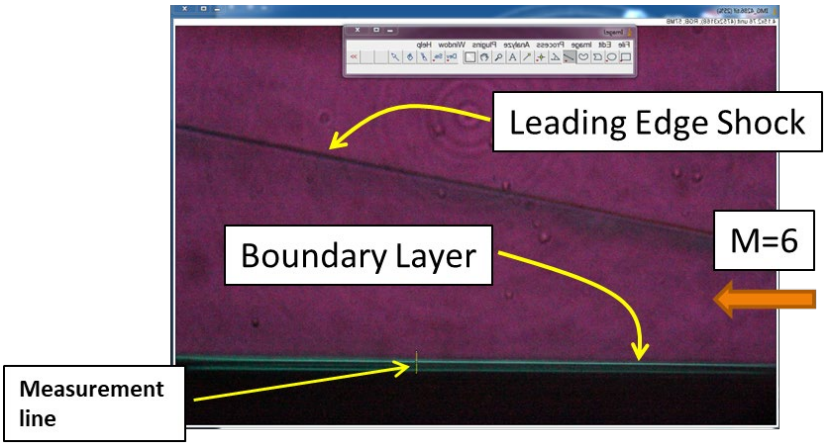

Figure 8 Example of two-color Schlieren to determine boundary layer thickness at the X = 7" station

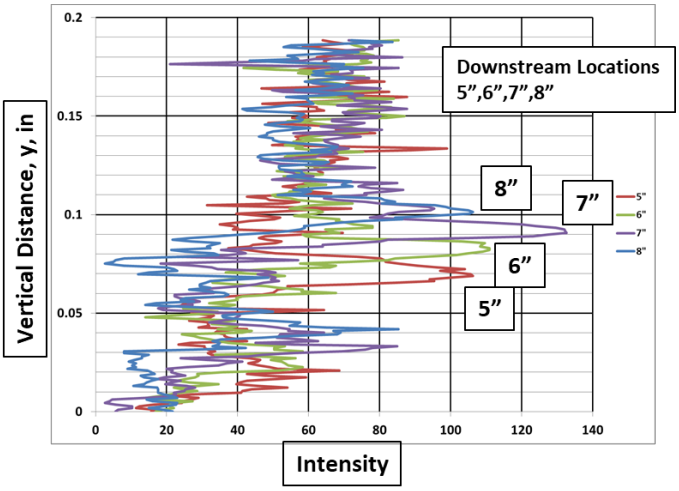

Figure 9 Vertical Distance vs. Intensity obtained from two-color Schlieren to determine boundary layer thickness at several X stations.

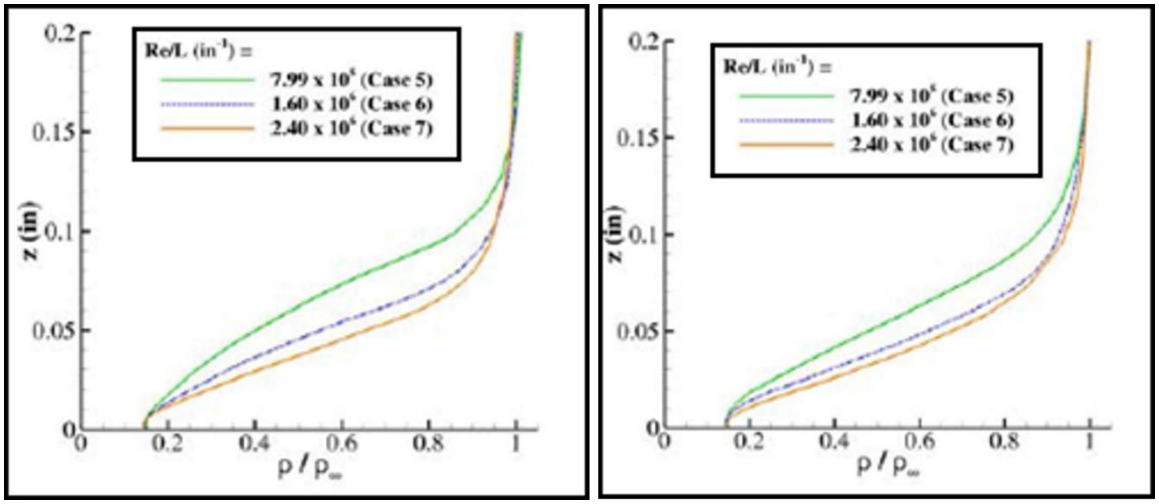

Figure 10 Example density profiles to estimate boundary layer thickness.

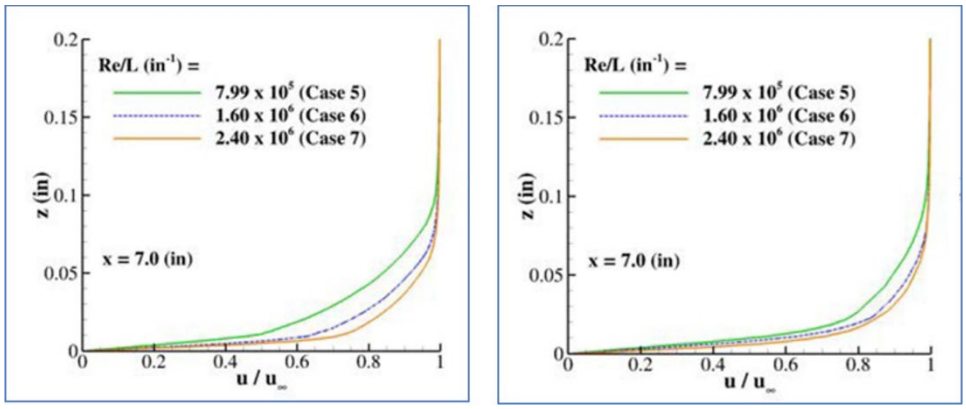

Figure 11 Velocity profiles from CFD at X = 7 inch station. Laminar (left) and turbulent (right) results shown.

A still image and single frame images from high speed video are presented in Figs. 12 and 13, respectively. The appearance of a protrusion on the leading edge is believed to be due to 3D effects Results from CFD developed prior to the execution of the experiments are presented in Fig. 14 and compared with experimental results for Cp and heat transfer rate. The laminar results for CFD are in reasonable agreement with experimental heat transfer upstream of the corner. The turbulent results for CFD are in reasonable agreement with experimental heat transfer downstream of the corner. The surface pressures from CFD are in reasonable agreement with the experimental data downstream of the corner.

Compression Ramp – Cold Wall data

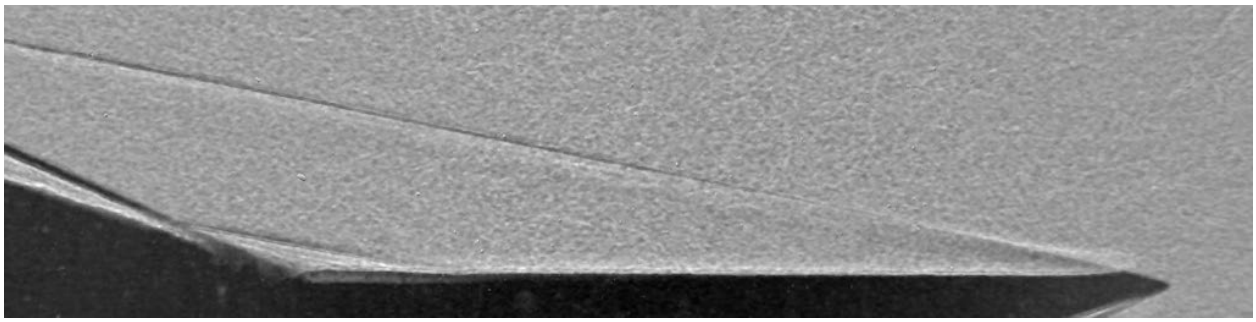

Figure 12 Example still image of shock boundary layer interaction - cold wall condition - Po = 700 psi.

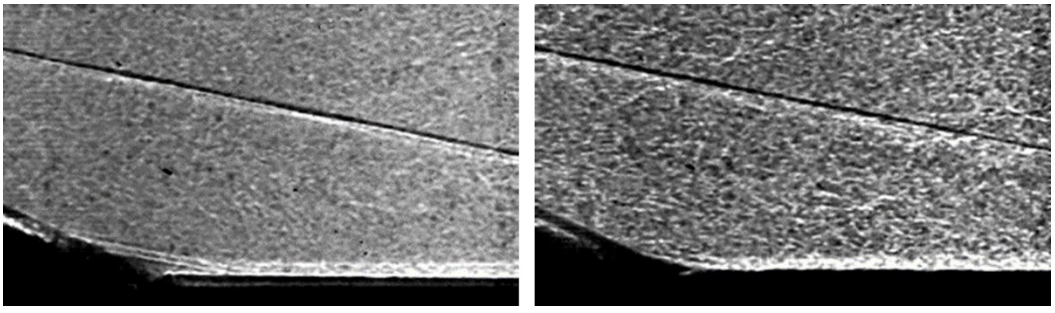

Figure 13 Example single frame images from high speed video. Results for Po = 700 (left) and Po = 2000 (right).

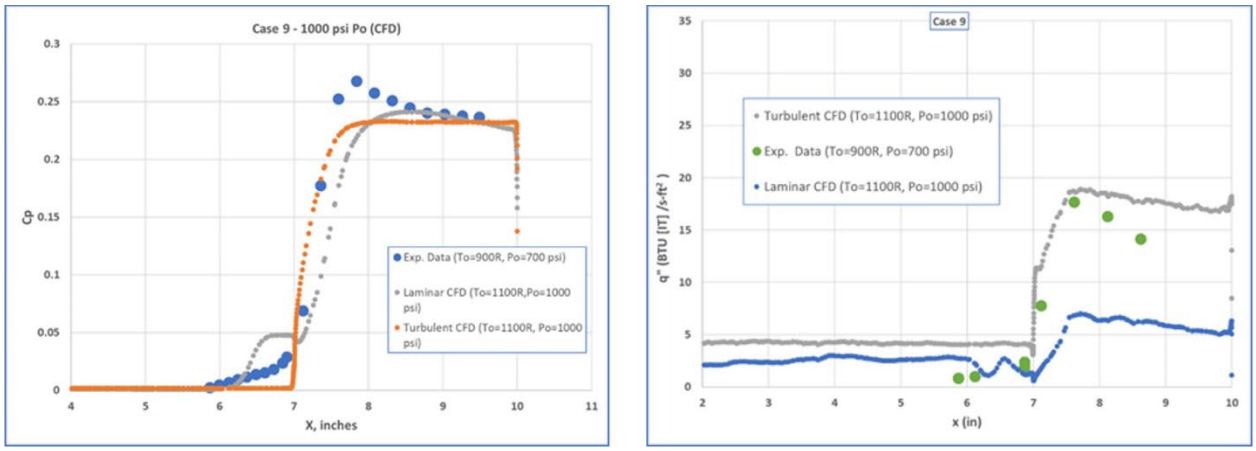

Figure 14 Cp vs. distance along centerline of model (left) and heat transfer (right) compared to laminar and turbulent CFD using pre-test conditions (CFD Re is 3% higher than experiment).

The centerline surface pressures are shown for the cold wall experimental data in Figs. 15-17. The closeup view in Fig. 17 is helpful when determining upstream influence locations. The results for the cold wall tests and the adiabatic wall tests are shown in Fig. 18. It is believed that the adiabatic wall condition causes boundary layer transition to occur earlier than the cold wall condition and thus the upstream influence distance is less than the cold wall case. Fig. 19 shows a close up view for determining upstream influence. The data from the 1400 Po and 700 Po runs are not shown in Fig. 19 and are still being reviewed.

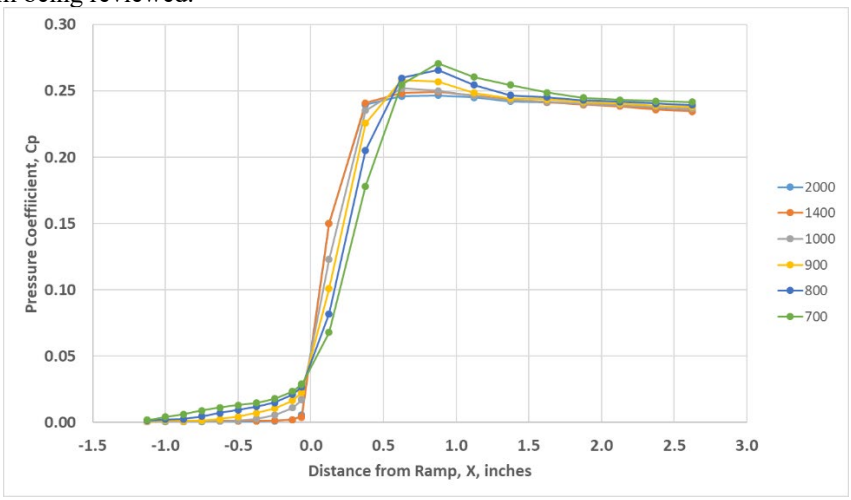

Figure 15 Pressure coefficient versus distance along centerline of model - cold wall data.

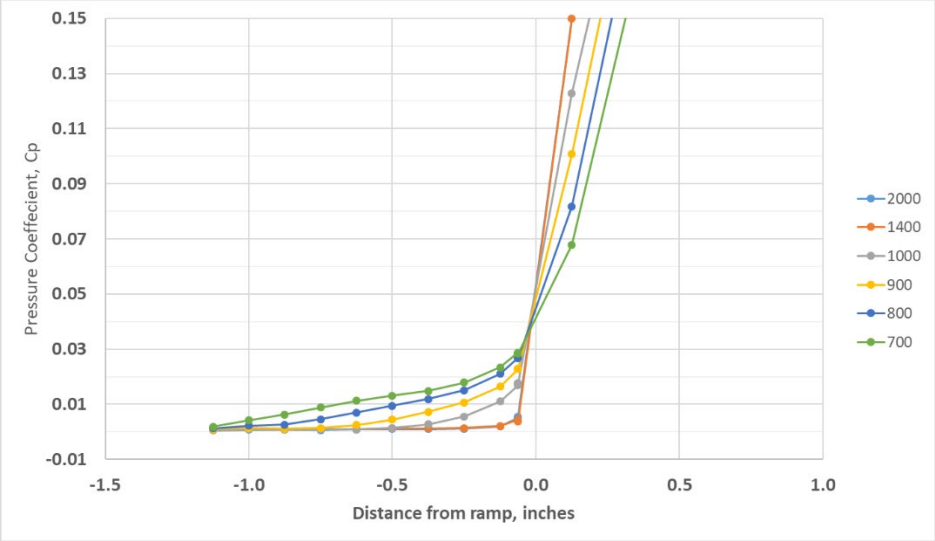

Figure 16 Pressure coefficient versus distance along centerline of model - closer view.

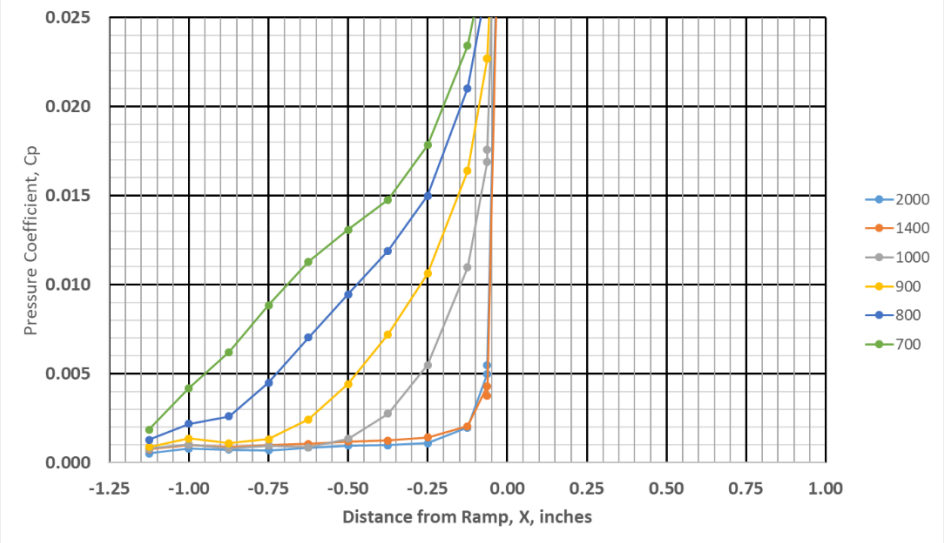

Figure 17 Pressure coefficient vs. distance along centerline of model - very close view.

B. Compression Ramp – Adiabatic Wall data

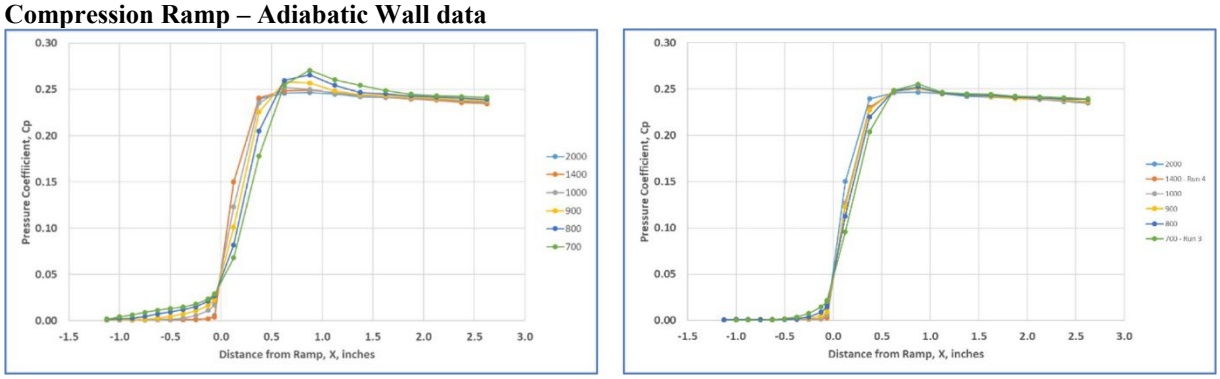

Figure 18 Pressure coefficient vs. distance along centerline of model for cold wall (left) and adiabatic wall (right) conditions.

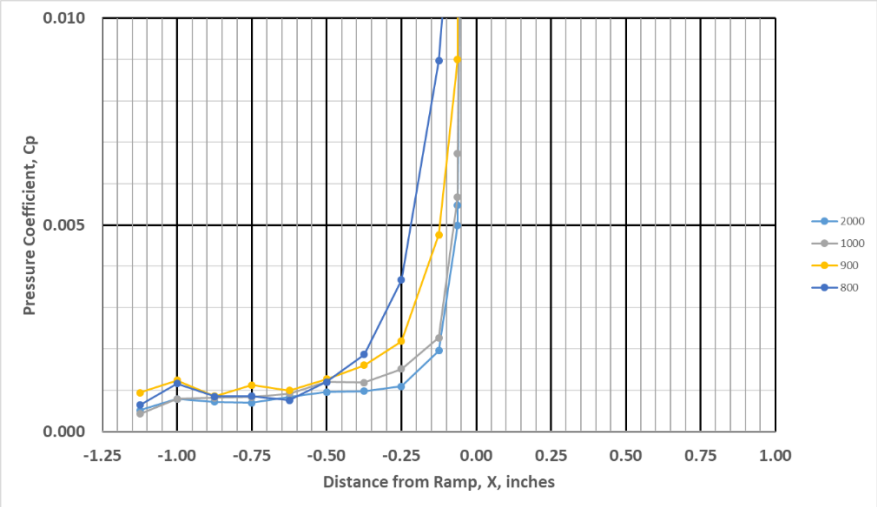

Figure 19 Pressure coefficient vs. distance along centerline of model - adiabatic data - close up view.

V. Scaling Methods

A. Similarity of Influence Lengths

Before discussing the scaling methods used in the present paper the author believes it would be appropriate to share some context on the state of the literature in this area. First, a quote from a paper published by Roshko and Thomke in 1976 [28] "It is curious that up to now there has been no cogent account of interaction length behavior in supersonic, turbulent boundary layers. … In a survey of over 100 papers and reports giving experimental results, we found it problematic to sort out trends." More recently, when discussing unsteady shock-induced turbulent separation, Dolling [6] states "Experiments from a wide range of facilities from continuous to intermittent, from transonic to hypersonic, have generated a data set that currently cannot be understood within a common framework." The author believes these two statements are at least partially true for supersonic and hypersonic flows with respect to upstream and downstream influence in laminar, transitional and hypersonic flows today.

It may be obvious to the reader, but it seems helpful to capture some of the reasons that a useful framework for upstream influence does not exist today. First, the upstream influence problem is often not the focus of research efforts that report it. This leads to anarchistic reporting practices where key quantities are not reported the same in the literature. For example, some researchers will report boundary layer thicknesses at the start of the interaction, while others report the boundary layer thickness at the same location but without the interaction. Additionally, the uncertainty associated with interpreting results from graphs can lead to different interpretations for the same data – especially when the normalized upstream influence is small. The definition of Reynolds number can also play a role – this is discussed later in the paper. Additionally, the presuppositions of the investigators may drive the filtering of results. For example, it was believed that there is no upstream influence in the flat plate portion upstream of a SBLI due to a compression ramp. However, it has been shown that favorable pressure gradients cause upstream influence [29] and this effect has been demonstrated in recent theoretical work [30,31]. In the present paper, we will try to make a first step toward a useful framework with respect to upstream influence and investigate downstream influence in future work.

In the present paper, we take a broad look at the determination of upstream influence. So broad that we require that any framework that hopes to capture upstream influence trends must be extensible to subsonic and even incompressible flows. This requirement then does not allow many supersonic theories [8,10,32] that have Mach numbers less than one to be considered. Lighthill [3] was the first to compare the upstream influence from incompressible to supersonic. While this theoretical approach has been a good foundation for work in the area since then, in this paper we take a much simpler approach. We consider the upstream influence problem to be driven by three types of forces – assuming adiabatic wall conditions: pressure forces, viscous forces with both scaled by inertia forces.

From incompressible boundary layer theory, Schlichting [33] describes a method by Von Kàrmàn and Pohlhausen [34] where a shape factor is defined as the ratio of pressure forces to viscous forces. This shape factor is defined as follows:

$$\Lambda = \frac{\delta^2}{\nu}\frac{dU}{dx} = -\frac{dp}{dx}\frac{\delta}{\mu U/\delta} \qquad \textbf{Eq. 1}$$

Looking at the right hand side and approximating the pressure gradient with:

$$\frac{dp}{dx} \cong \frac{\Delta p}{\delta} \qquad \textbf{Eq. 2}$$

we have assumed that the local change in pressure in the axial direction occurs over a distance on the order of one boundary layer thickness. For typical laminar boundary layers encountering a SBLI, this approximation for the local pressure gradient seems reasonable if the boundary layer thickness is taken as either upstream of the interaction or fixed and based on the undisturbed value at the compression corner (for example). For turbulent flows it may require the addition of a constant since the pressure changes over one boundary layer thickness may be more nonlinear since the entire interaction may occur only in 1-2 boundary layer thicknesses in length.

Rearranging Eq. 1 and substituting for the pressure gradient yields:

$$\Lambda \cong -\frac{\Delta p}{\delta}\frac{\delta}{\mu U/\delta} = -\frac{\Delta p}{\rho U^2}\frac{\rho U \delta}{\mu} \qquad \textbf{Eq. 3}$$

$$\Lambda \cong -\frac{C_p}{2} Re_\delta \qquad \textbf{Eq. 4}$$

While this quantity has been developed for local phenomenon in incompressible flow, in Ref. [35] a global perspective in supersonic flow is considered where Δp is now interpreted as the inviscid change in pressure causing the SBLI. In that case, the result for the ratio of pressure forces to viscous forces is of the form $\frac{Re\, C_p}{2}$, where the Reynolds number is based on the running length. For lack of a better term, we call this quantity an "interaction parameter" hopefully not to be confused with the hypersonic viscous interaction parameter which is often used in the analysis of leading edge shocks over flat plates.

A brief review of the background of the interaction parameter follows. Restricting our discussion to the 2D compressible momentum equation in the Cartesian x direction [36]:

$$\frac{\partial \rho u}{\partial t} + \frac{\partial}{\partial x}[\rho u^2 + p - \tau_{xx}] + \frac{\partial}{\partial y}[\rho u v - \tau_{xy}] = 0$$

with

$$\tau_{xx} = \frac{2}{3}\mu\left(2\frac{\partial u}{\partial x} - \frac{\partial v}{\partial y}\right);\ \tau_{xy} = \mu\left(\frac{\partial u}{\partial y} + \frac{\partial v}{\partial x}\right)$$

The nondimensionalization approach is detailed below with nondimensional quantities annotated with a tilde:

$$\tilde{x},\ \tilde{y} = \frac{x}{L}, \frac{y}{L};\ \tilde{t} = \frac{t}{L/V_\infty};\ \tilde{\rho} = \frac{\rho}{\rho_\infty};\ \tilde{u}, \tilde{v} = \frac{u}{V_\infty}, \frac{v}{V_\infty};\ \tilde{p} = \frac{p}{\Delta p}$$

There is nothing unusual about this approach to nondimensionalization, except for the pressure. In this approach the pressure is nondimensionalized by a change in pressure that is representative of the interaction causing the formation of the influence region (which is a region that can be decoupled from the rest of the flowfield computationally [35]). For two dimensional supersonic flows where a geometric turning angle is known, the representative pressure change can be determined analytically. It was shown in Ref. [35] that using the above nondimensionalization the equations can be written with a similarity variable of the form, $\frac{Re\,\Delta p}{\gamma M_\infty^2 p_\infty}$, or a more general form of $\frac{Re\, C_p}{2}$,, where the pressure coefficient is defined in the usual way in terms of the reference change in pressure

and the freestream dynamic pressure. This parameter becomes a leading coefficient of the pressure gradient term in the momentum equation when using the nondimensionalization above and grouping it with the shear stress term. Similar parameters have been mentioned as representing the ratio of pressure forces to viscous forces (Ref. [37]). In the present paper we use $\frac{Re\, C_p}{2}$ to characterize all upstream influence normalized with respect to the undisturbed boundary layer thickness at the source of the interaction – for a compression ramp this location would be at the flat plate / ramp juncture. We also note that downstream influence could be characterized in a similar way, but we will leave downstream influence research for future work.

An important assumption in the present paper is that we must adopt a consistent basis for reporting normalized upstream influence. Another key assumption is the definition of Reynolds number used for scaling. Here we use the traditional definition based on a running length which is better suited for system level understanding of influence regions and their limits of influence. The last of these two assumptions helps to interpret turbulent flows on a more consistent basis. It is also important to note that the choice of Reynolds number definition can have an impact on the ability to see important trends in turbulent data. Roshko and Thomke [28] point out that it is possible to compress a larger Reynolds number range into a smaller one through the use of Cf. It is believed that using a Reynolds number based on running length with give the greatest insight and lowest uncertainty for understanding trends in upstream and downstream influence.

Therefore when turbulent upstream influence is reported in the literature in other Reynolds number quantities (such as boundary layer Reynolds number, displacement thickness Reynolds number, momentum thickness Reynolds number, etc…) we convert those Reynolds numbers to a Reynolds number based on the running length of an equivalent flat plate. When necessary, the correlation developed by Ramesh and Tannehill [38] is used for this purpose:

$$\frac{\delta}{x} = \frac{0.36\, C_w^{0.2}}{Re_x^{1/7}} [\, 0.4444 - (0.02625\, M_\infty^{0.1}) - 0.0005\, M_\infty\, (6 - M_\infty^{1.1})] \qquad \textbf{Eq. 5}$$

$$C_w = (\frac{T_{aw}}{T_\infty})^{-1/3} \qquad \textbf{Eq. 6}$$

These correlations have been compared to experiments [38] and have been stated as accurate for Mach numbers 2.5 to 5.0 and Reynolds number per meter of 3.32E6 to 1.11E8. We consider this correlation to be a reasonable approximation for the purposes of this paper that require computation of the boundary layer thickness for turbulent flow.

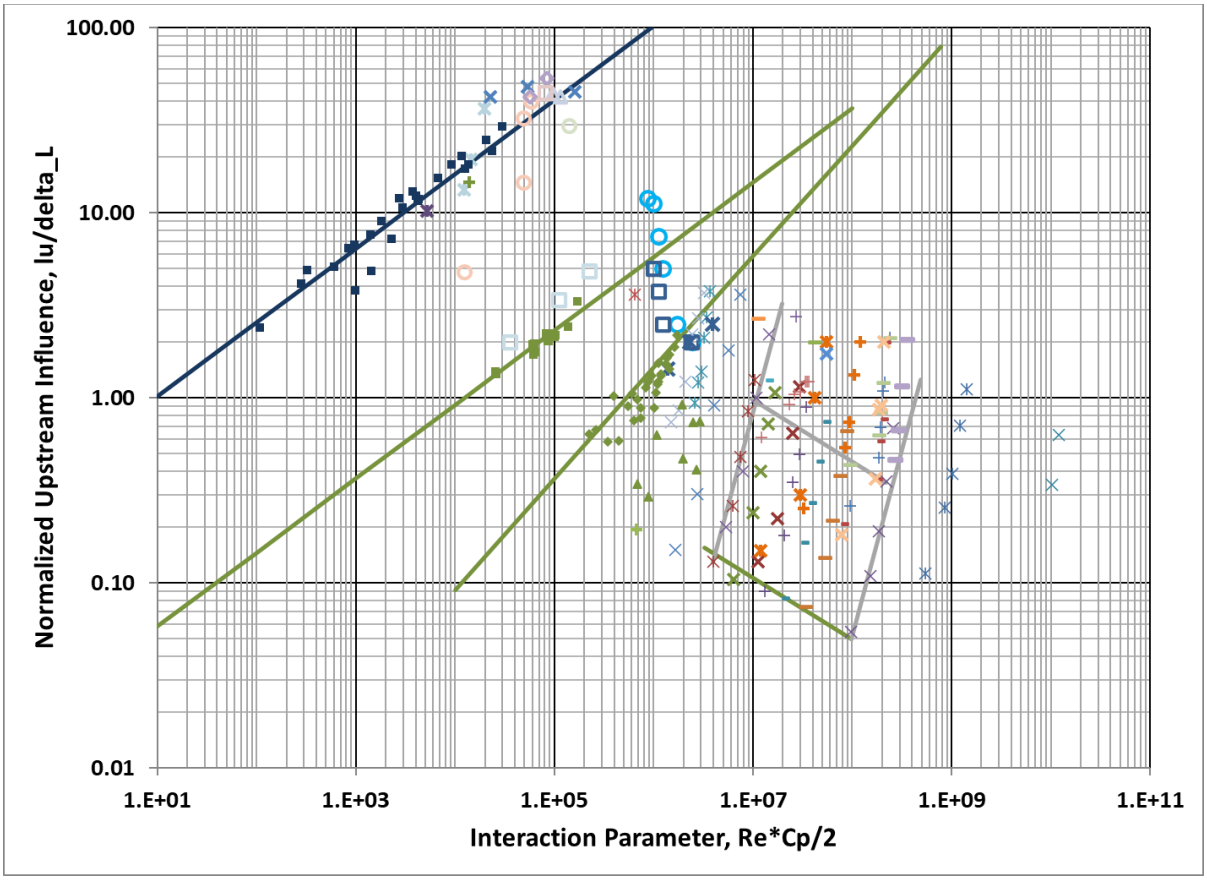

Figure 20 Normalized upstream influence vs. interaction parameter for laminar, transitional and turbulent flows. Legend for data is shown in next Figure.

The complete set of data considered for the present paper are shown in Fig. 20 with a legend in Fig. 21. The complete set is complicated to interpret, so smaller categories of data will be used to discuss the data later in the paper. Tabular data corresponding to the datasets in the figure are included in the Appendix. Generally speaking: the solid symbols represent numerical data for laminar or RANS (Reynolds Averaged Navier-Stokes) results for turbulent; the open bounded symbols are transitional data (either experimental or numerical); and the open unbounded symbols are experimental data for laminar or turbulent flows and includes high fidelity CFD such as Direct Numerical Simulation (DNS).

Figure 21 Legend for data shown in previous figure.

In this figure [Fig. 20 and 21], it is clear that the upstream influence generally increases with interaction parameter, but the slope of the upstream influence appears to be a function of Reynolds number for turbulent flows, while for laminar flows the upstream influence varies with the interaction parameter raised to the 2/5 power. It should be noted that the vast majority of the data sets include changes to ramp angle while holding Re and Mach constant. For turbulent flows, Settles et al. [39] has shown that the effects of Reynolds number scale with $(Re_\delta)^{-1/3}$. More investigation is needed to explore the effects of Mach number and Reynolds number independently. The exponent derived from recent theoretical investigations using scaling patch analysis seems to indicate a ½ power [40-42] for viscous flows. The multi-valued results for upstream influence are similar in character to that of incompressible pipe flow and the Moody diagram [43] where the friction factor varies at constant slope with Reynolds number independent of pipe roughness, while for turbulent flow, the slope depends on pipe roughness. It is interesting to note that the length/diameter ratio for incompressible laminar flow through a pipe is equal to $\frac{Re\, C_p}{2}$ to within a constant [43].

Based on a review of the data in this figure, there appears to be several types of trends. They will be presented in later figures individually, and summarized here:

I. *Laminar*
- This set of data has a large number of numerical values presented in [29]. Experimental data has also been included [4,12,44,45]. Some experimental values reported in [29] were removed because they contained data for forward facing steps and not compression ramps.

II. Transitional
- *Laminar-like*
  - This set of data contains transitional flow as reported by the authors, but the upstream influence clearly falls on the laminar trend line [4,12,15,17,18]. It is believed that much of this data represents transitional behavior only near the reattachment point and not in the majority of the SBLI.
- *Transitional*
  - Currently we see this as having only one data set – that of Gray and Rhudy [12]. More investigation is needed to characterize this region.
- *Turbulent-like*
  - Similar to the wording for the "Laminar-like" category, this set of data is reported as transitional but appears to fall on the low to mid Re Turbulent category. The present experimental results appear in this category and the data of Whalen et al. [16].

III. Low Re Turbulent
- This data set has all numerical data from RANS computations [38] except for one data point [46]. The Reynolds number range for the numerical data is from 1.0E6 to 1.7E6 and the Mach number range is from 2.5 – 5.0. The numerical data was validated with some experimental data in the Mid Re range of conditions studied. The interesting observation about this category is that the slope of this trend is the same as observed for laminar flow (2/5).

IV. Mid Re Turbulent
- This data set also has a majority of numerical data from RANS computations [38] except for a couple of experimental data sets at Mach 1.5 [47] and Mach 2.94 [48]. The Reynolds number range for the numerical data is from 4.6E6 to 1.0E7 and the Mach number range is from 2.5-4.5. The numerical data was validated with some experimental data in the range of conditions studied. The slope of this trend line is slightly higher (3/5).

V. High Re Turbulent
- This data set consists of numerical data from RANS computations [38] and experimental data that does not follow a Cp^2 trend (discussed in the next category) [49-55] or is limited in number and not sufficient to establish a trend. The Reynolds number range for the numerical data in this category is from 1.3E7 to 3.2E7, and the Mach number is 2.96.

VI. Inviscid Dominated Turbulent with Cp^2 trend
- The last category is motivated by the recent scaling of Souverein et al. [56] which has been recently extended to axisymmetric cone/flare geometries [57]. All of the data from Settles et al. [39] and much of the data from Roshko and Thomke [49] fall into this category. The data of Law [48] could also be included in this category but is listed in the Mid Re category because of the proximity to the mid Reynolds number numerical data. More investigation of this is left for future work. More discussion of this Cp^2 scaling and other scaling approaches for turbulent flows follow.

B. Analysis of Souverein et al. [56] Scaling for Turbulent Interactions

In Ref. [56] a scaling for the interaction length is based on a mass balance taken around the SBLI region. It results in the following form:

$$L^* = 1.3 * [S_e^*(Re_\theta)]^3 \qquad \textbf{Eq. 7}$$

where

$$L^* = \frac{L}{\delta^*_{in}}\, G_3;\; G_3 = \frac{\sin(\beta)\sin(\varphi)}{\sin(\beta-\varphi)} \qquad \textbf{Eq. 8}$$

It is important to note that the right-hand side of the second equation in Eq. 8 has some common factors with the pressure coefficient when considering a compression ramp in an inviscid flow [58]. Using this observation, the quantity G_3 can be written in terms of a pressure coefficient and the tangent of the difference between the shock angle and the ramp angle. In the Figure below (Fig. 22), it is important to note that the tangent term is nearly independent of turning angle. This leaves the dependence on turning angle restricted to the Cp term.

$$G_3 = \frac{C_p}{2}\,\frac{1}{\tan(\beta-\varphi)} \qquad \textbf{Eq. 9}$$

From Ref. [56], the definition of the separation interaction strength variable is given by:

$$S^*_e = k\,C_p; k = \begin{cases} 3 & if\ \ Re_\theta < 10{,}000 \\ 2.5 & if\ \ Re_\theta \geq 10{,}000 \end{cases} \qquad \textbf{Eq. 10}$$

Rewriting Eq. 7 with the substitutions from Eq. 9 and Eq. 10 yields an alternative form for the scaling:

$$\frac{L}{\delta^*_{in}} = \tan(\beta-\varphi)\,2.6\,k^3\left(C_p\right)^2 \qquad \textbf{Eq. 11}$$

Some observations about this scaling are appropriate. It is apparent from the equation that the upstream influence is a

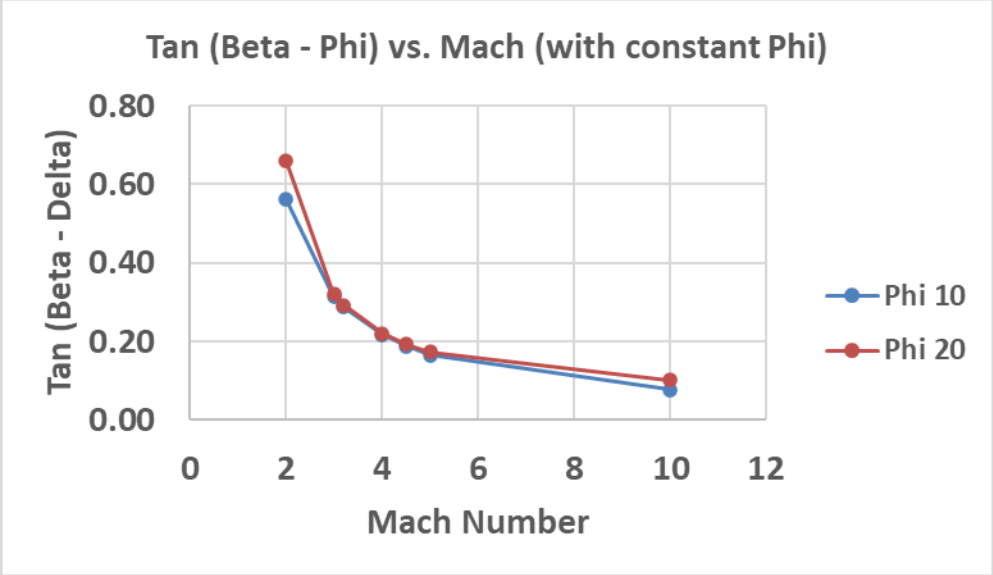

Figure 22 Tan (beta - phi) vs. Mach number

function of the Mach number and geometry of the compression ramp with a weak dependence on Reynolds number. This seems counter-intuitive when one would expect a Reynolds number dependence to be more obvious since the left hand side contains the displacement thickness. Nevertheless the references that justify the independence of momentum thickness Reynolds number are quoted in Ref. [56] and had been documented elsewhere in the literature. This independence is based on the incipient separation angles for turbulent interactions.

However it is not clear that the normalized upstream influence will follow the same independence of momentum thickness Reynolds number as the incipient separation angle. For example, the data of Settles and Bogdonoff [59] show that the normalized upstream influence is a strong function of boundary layer thickness Reynolds number. The correlation presented in that work accurately predicts the trends from [59] as well as the work of Law [48] and Roshko

and Thomke [49] based on a boundary layer thickness formulation for Reynolds number. In addition, Fig. 5 of Frew et al. [18] show that the incipient separation angle for several experimental conditions decreases with increasing boundary layer thickness Reynolds number while the data of Law [48] and Roshko and Thomke[49] show that the incipient separation angle increases with increasing boundary layer thickness Reynolds number. Based on the limited momentum thickness Reynolds number range of the Souverein et al. [56] data, we conclude that the momentum thickness Reynolds number effects on upstream influence described in that scaling are in a limited range when evaluated in terms of a running length Reynolds number.

C. Analysis of Roshko and Thomke (July 1976) Scaling [28]:

The scaling of Roshko and Thomke was applied to a Mach number range from 1.98 to 4.93 and is given below.

$$\frac{l_0}{\delta_0} = \sigma\left(C_{f0} - C_{f0}^{*}\right);\ \sigma = 10^3\left(\frac{\alpha}{18.29}\right)^{2.81} \qquad \textbf{Eq. 12}$$

Note that the dependence on Reynolds number comes through the skin friction coefficient and inviscid effects are determined by a single geometric parameter – the ramp angle. In their paper, Roshko and Thomke state that "when l_0/δ_0 is plotted against Cf_0, the data for different values of Mach number (excluding the M_e = 1.98 data) fall onto a single curve for each value of α". This statement seems to imply an independence of Mach number. An observation from the variation of Cp with Mach number can be developed from the Figure below:

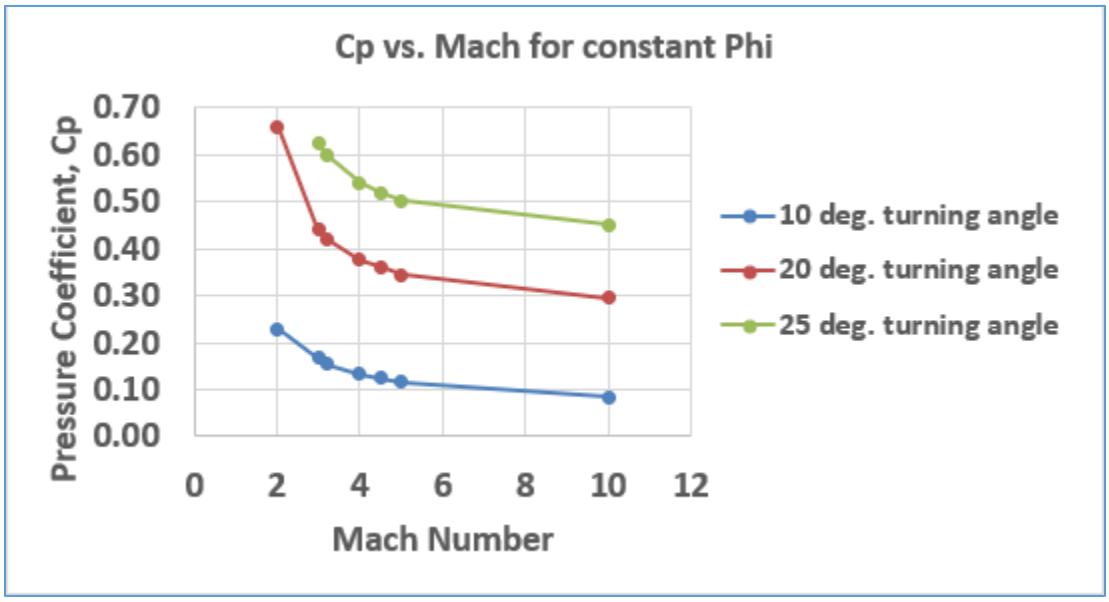

Figure 23 Pressure Coefficient vs. Mach for constant turning angle, phi

From this figure it is clear that the change in Cp decreases rapidly once the Mach number gets above about 3. The relative change then also decreases as the ramp angle increases. This helps to explain the earlier statement in [28]. The author is not aware of any other work to explain this observation.

D. Discussion of Settles (1982) scaling[39,59-61]:

The data of Settles et al. [39] has been well-characterized by the following scaling equation.

$$\frac{L_m}{\delta_0} = \frac{1}{Re_{\delta_0}^{1/3}} 0.9\ e^{0.23\,\alpha} \qquad \textbf{Eq. 13}$$

This scaling also captures the trends in other data sets such as Roshko and Thomke [28,49]. It is also important to note that the trend in boundary layer thickness Reynolds number (-1/3 exponent) also holds when representing the data in terms of a running length Reynolds number as shown later in Fig. 29.

E. Discussion of Ramesh and Tannehill (2001) scaling [38]:

This scaling was developed from a numerical study using RANS simulations. The RANS data was validated with a few experimental data points and also compared to Navier-Stokes computations. The data from that study provides the vast majority of turbulent data in the "Low" and "Mid" Re categories.

$$\frac{l_u}{\delta_L} = 48\,\frac{\exp(0.1\,\theta + M_\infty^{0.3})}{\left(Re_{\delta_L}\right)^{5/9}} \qquad \textbf{Eq. 14}$$

F. Graphical Results for Categories of Upstream Influence

In the following Figures, the entire data set is presented in smaller categories to clarify the trends in the data.

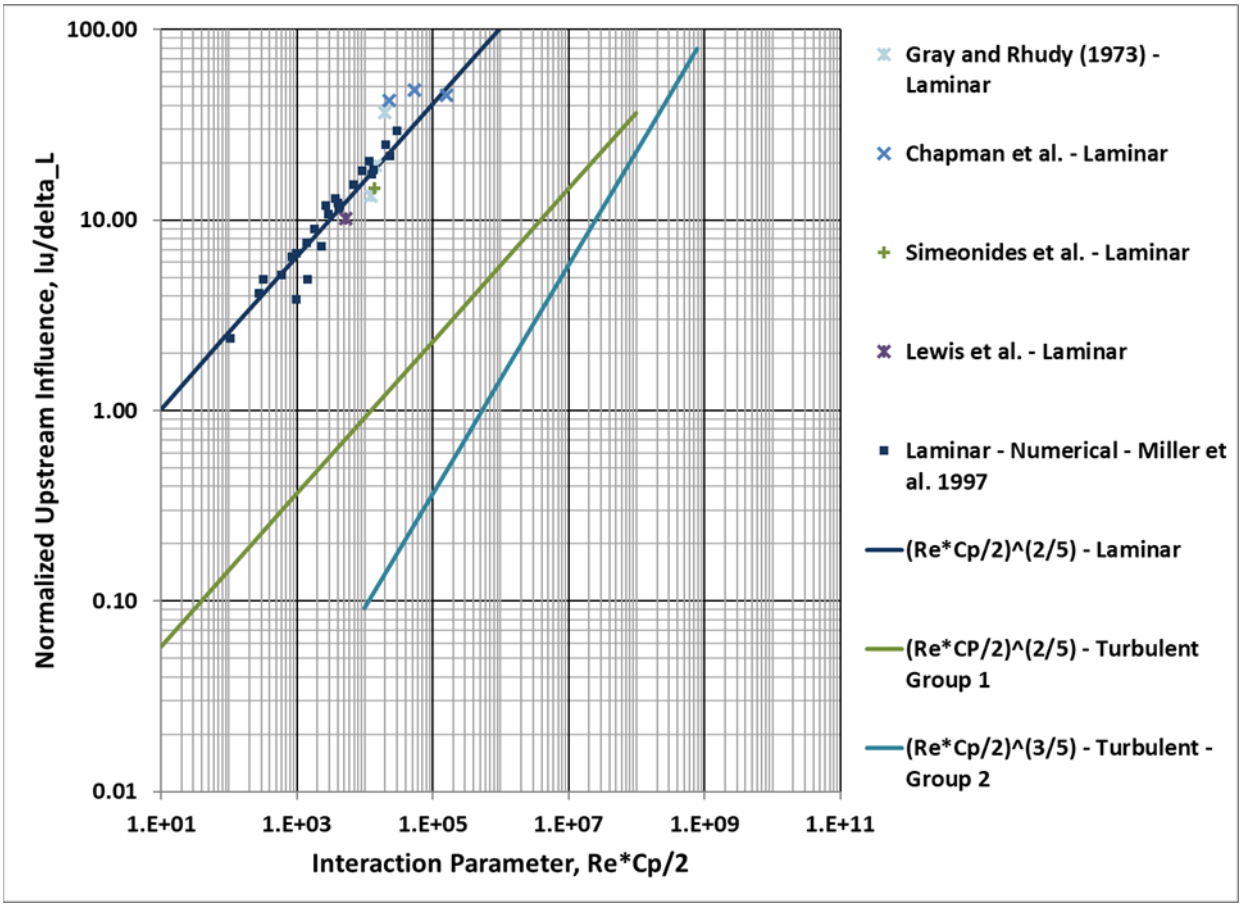

Figure 24 Laminar Category of Upstream Influence

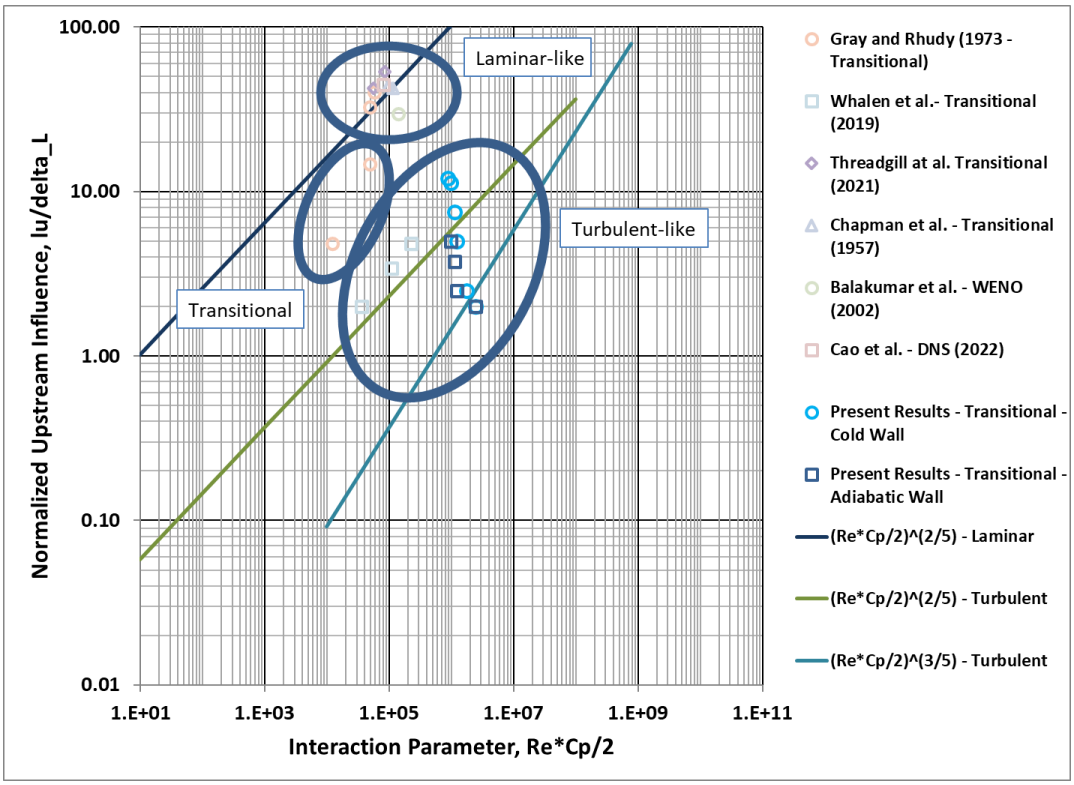

Figure 25 Transitional, with several sub-categories: Laminar-like, Transitional, Turbulent-like. Note that the data of Whalen et al., Balakumar et al., and Cao et al. are for cold wall conditions. Their normalized upstream influence is expected to decrease for adiabatic wall conditions as described in the text.

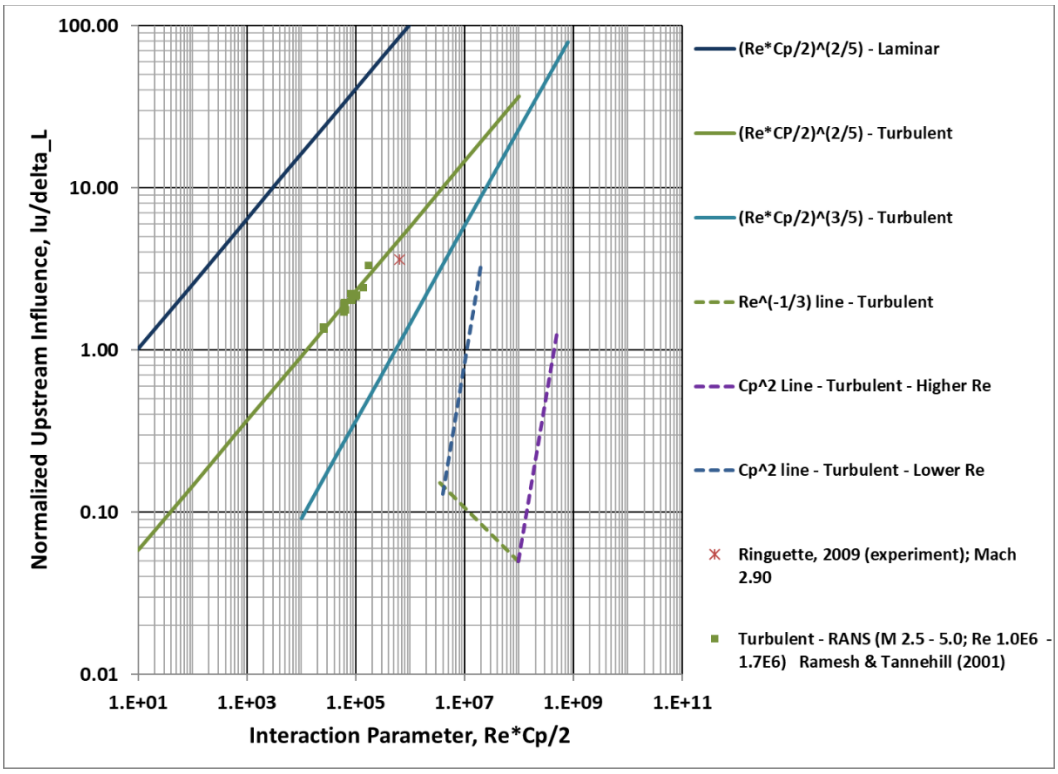

Figure 26 Low Reynolds number - turbulent category. The slope for this category is also (2/5) as in the laminar category.

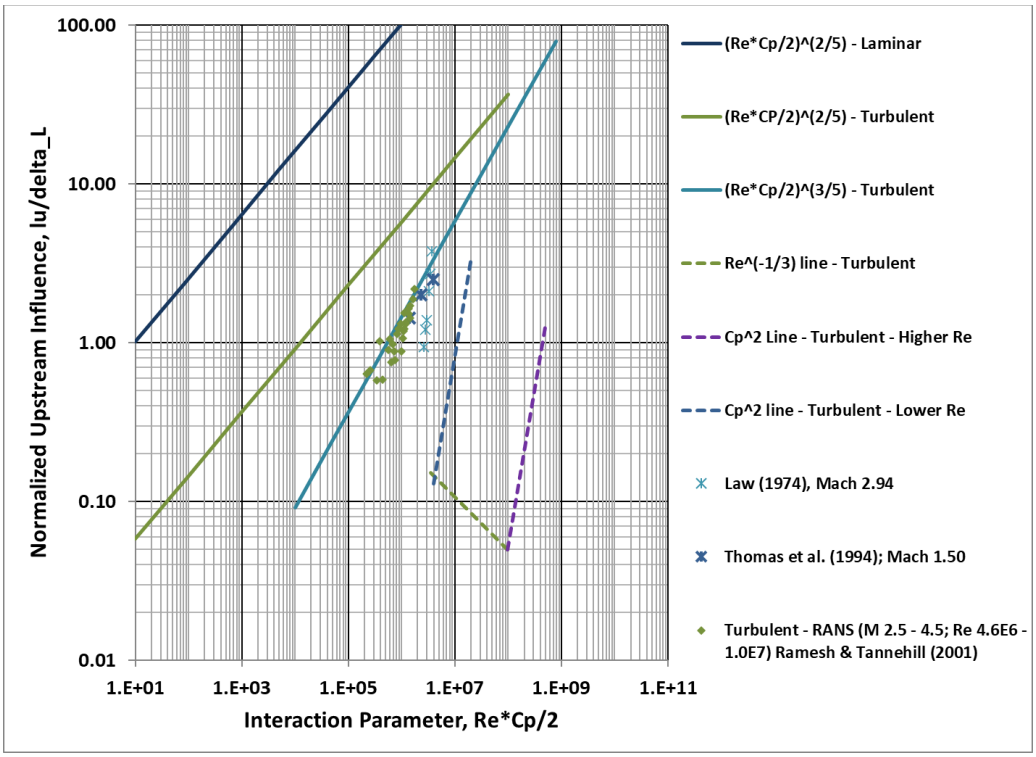

Figure 27 Mid Reynolds number category. The slope for this category is (3/5) based on numerical data. Note that the data of Law (1974) has a strong Cp^2 trend as in the last category (Category VI – Inviscid-dominated with Cp^2 trend).

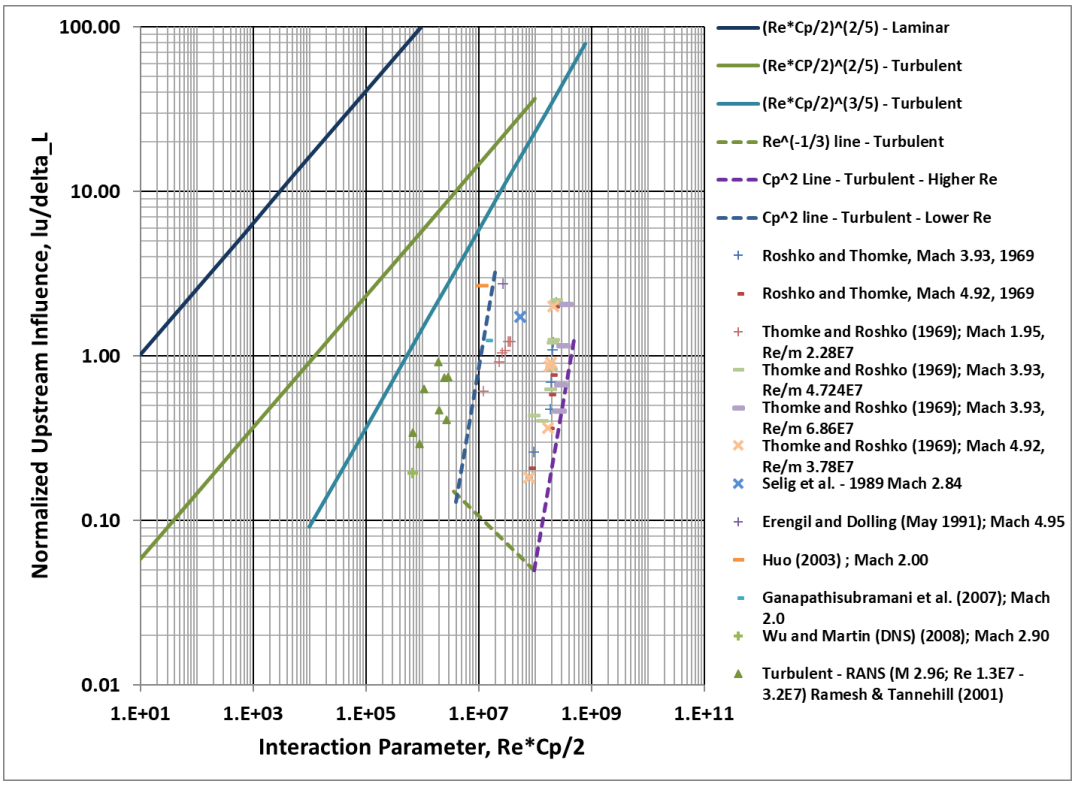

Figure 28 High Reynolds Number – turbulent category. This category includes numerical data and data that does not fit the Cp^2 trend or is not sufficient to establish a trend.

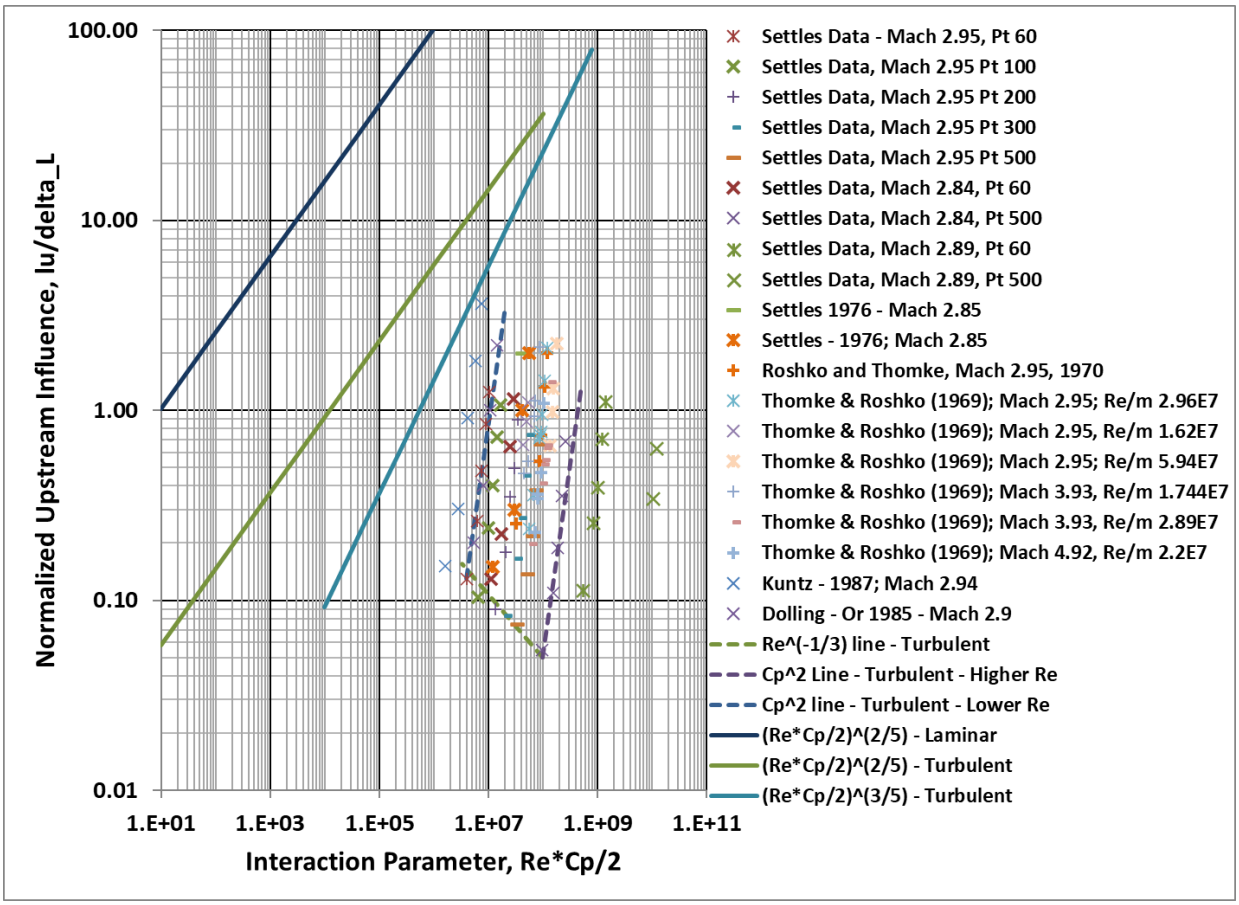

Figure 29 Inviscid Dominated Turbulent with Cp^2 trend category. This category is based on the inviscid Cp^2 scaling of Souverein et al. and includes a strong dependence on Reynolds number developed by Settles and Bogdonoff [39].

VI. Conclusion

Experimental results have been presented for a transitional Mach 6 flow over a flat plate and compression ramp geometries. Unsteadiness and heat transfer results are consistent with other investigations of this type. In addition, a new framework for understanding upstream influence was discussed. Upstream influence appears to have several categories of data even for an adiabatic wall assumption. Laminar, transitional and turbulent scaling of these interactions are described on a consistent basis by using a running length Reynolds number for all datasets. As much of the data is limited to changing compression ramp angles while keeping Reynolds number and Mach number constant, the bulk of the trends can be understood in terms of changing compression ramp angle. The slope of these trends depends strongly on Reynolds number or Cp and the category of the upstream influence interaction.

Appendix

Table 1 Gray and Rhudy (1973) - Laminar

Mach	Re_xc	Delta L (in.)	lu	lu/Delta L	P2/P1	Cp/2	Re*Cp/2
3	2.50E+05	3.84E-02	1.408	36.67	1.987215	0.07835	1.96E+04
4.5	2.50E+05	5.43E-02	1.050	19.35	2.6416	0.057905	1.45E+04
6	2.50E+05	7.51E-02	1.000	13.31	3.469251	0.048993	1.22E+04

Table 2 Chapman et al., Laminar

Mach	Re_L	L,m	delta_p/p	Re*Cp/2	lu/delta_L	Delta(mm)
2.00	1.80E+05	0.0572	0.71	22821.43	42.42	0.836
2.00	4.20E+05	0.0572	0.71	53250	48.08	0.547
2.00	1.26E+06	0.0572	0.71	159750	45.25	0.316

Table 3 Simeonides, Laminar

Mach	Re_L	Re*Cp/2	delta_p/p	L,m	lu/delta_L
6.00	4.00E+05	13888.89	1.75	0.04	14.70

Table 4 Lewis - Laminar

Mach	Re_L	Re*Cp/2	delta_p/p	L,m	lu/delta_L
6.06	1.50E+05	5251.59	1.8	0.0635	10.20

Table 5 - Laminar CFD - Miller et al. (1997)

Cp/2	Mach	Re_L	Re*Cp/2	delta p/p	L, m	lu/L	lu/Delta_L
0.0607	2.00	1.50E+05	9,107.1	0.34	0.0635	0.291	18.18
0.0125	2.00	2.96E+05	3,700.0	0.07	0.0490	0.150	12.98
0.0393	2.00	2.96E+05	11,628.6	0.22	0.0490	0.232	20.35
0.0696	2.00	2.96E+05	20,614.3	0.39	0.0490	0.283	24.82
0.1000	2.00	2.96E+05	29,600.0	0.56	0.0490	0.334	29.29
0.0091	2.50	2.96E+05	2,706.3	0.08	0.0490	0.151	11.96
0.0229	2.50	2.96E+05	6,765.7	0.20	0.0490	0.194	15.36
0.0457	2.50	2.96E+05	13,531.4	0.40	0.0490	0.231	18.28
0.0800	2.50	2.96E+05	23,680.0	0.70	0.0490	0.273	21.61
0.0063	3.00	1.68E+04	106.7	0.08	1.0000	0.145	2.40
0.0167	3.00	1.68E+04	280.0	0.21	1.0000	0.250	4.13
0.0357	3.00	1.68E+04	600.0	0.45	1.0000	0.310	5.12
0.0579	3.00	1.68E+04	973.3	0.73	1.0000	0.405	6.69
0.0841	3.00	1.68E+04	1,413.3	1.06	1.0000	0.460	7.60
0.0063	3.00	5.04E+04	320.0	0.08	3.0000	0.167	4.88
0.0167	3.00	5.04E+04	840.0	0.21	3.0000	0.220	6.43
0.0357	3.00	5.04E+04	1,800.0	0.45	3.0000	0.307	8.98
0.0579	3.00	5.04E+04	2,920.0	0.73	3.0000	0.367	10.73
0.0841	3.00	5.04E+04	4,240.0	1.06	3.0000	0.407	11.90
0.0270	3.00	1.50E+05	4,047.6	0.34	0.0635	0.244	12.31
0.0167	3.00	2.52E+05	4,200.0	0.21	15.0000	0.177	11.56
0.0167	3.00	7.56E+05	12,600.0	0.21	45.0000	0.153	17.33
0.0152	4.00	1.50E+05	2,276.8	0.34	0.0635	0.181	7.25
0.0095	5.05	1.50E+05	1,428.4	0.34	0.0635	0.154	4.86
0.0066	6.06	1.50E+05	992.0	0.34	0.0635	0.150	3.82

Table 6 Gray and Rhudy (Transitional) (1973)

Mach	Re_xc	Delta L (in.)	lu/Delta L	P2/P1	Cp/2	Re*Cp/2
4.5	1.00E+06	2.71E-02	40.18	2.6416	0.057905	5.79E+04
6	2.50E+05	7.51E-02	4.82	3.469251	0.048993	1.22E+04
6	1.00E+06	3.76E-02	14.64	3.469251	0.048993	4.90E+04
6	1.00E+06	3.76E-02	32.60	3.469251	0.048993	4.90E+04

Table 7 Whalen et al. (2019) - Transitional

Ramp angle - Table 6	Mach	Re/m (Table 1)	Re_L	Re*Cp/2	Cp/2	P2/P1	Delta_L (mm) (Table 1)	lu/Delta L (Fig. 5a)
10	5.96	6.60E+06	6.73E+05	3.58E+04	0.05311	3.64109	4.55	2
20	5.96	6.60E+06	6.73E+05	1.10E+05	0.16389	9.15008	4.55	3.4
30	5.96	6.60E+06	6.73E+05	2.24E+05	0.33292	17.556	4.55	4.84

Table 8 Threadgill et al. (2021)

Ramp angle - Table 6	Mach	Re/m (Table 1)	Re_L	Re*Cp/2	Cp/2	P2/P1	Delta_L (mm) (Table 6)	lu/Delta L
22	3.88	4.56E+06	2.55E+05	5.66E+04	0.22202	5.6793	0.82	42.19512
28	3.88	4.56E+06	2.55E+05	8.43E+04	0.33059	7.9675	0.73	53.42466

Table 9 Chapman - Transitional

Mach	Re_L	Re*Cp/2	delta_p/p	L,in	lu/delta_L
2.70	1.05E+06	9.639E+04	0.936907	2.25	44.26
2.60	3.30E+05	1.143E+05	3.277864	5	42.42

Table 10 Balakumar et al. (Transitional)

Mach	Re/ft (Fig. 1)	Re_L	Re*Cp/2	Cp/2	P2/P1	Delta_L (in) (Fig. 6)	lu/Delta L
5.373	5.46E+06	5.67E+06	1.39E+05	0.02459	1.99382	0.076	29.53947

Table 11 Cao et al. (Transitional)

Mach	Re*Cp/2	Cp/2	P2/P1	Pg. A8-4: L (mm)	Re_L	Delta_L/L	Fig. 4 lu/L	lu/Delta L
7.70	8.04E+04	0.09351	8.76172	100	8.60E+05	1.35E-02	0.6	4.45E+01

Table 12 - Present Experimental results - 16 deg. compression ramp – cold wall and adiabatic wall cases

Mach	Re_L	Re*Cp/2	delta_p/p	lu/delta_L	P0 (psi)	Wall Temperature
5.85	7.64E+06	8.631E+05	5.413	12.00	700	Cold Wall
5.85	8.73E+06	9.864E+05	5.413	11.25	800	Cold Wall
5.85	9.82E+06	1.110E+06	5.413	7.50	900	Cold Wall
5.85	1.09E+07	1.233E+06	5.413	5.00	1000	Cold Wall
5.85	1.53E+07	1.726E+06	5.413	2.50	1400	Cold Wall
5.85	2.18E+07	2.466E+06	5.413	2.00	2000	Cold Wall
5.85	8.73E+06	9.864E+05	5.413	5.00	800	Ad. Wall
5.85	9.82E+06	1.110E+06	5.413	3.75	900	Ad. Wall
5.85	1.09E+07	1.233E+06	5.413	2.50	1000	Ad. Wall
5.85	2.14E+07	2.417E+06	5.413	2.00	1960	Ad. Wall

Table 13 Wu and Martin - DNS (2008)

Ramp angle (deg)	Re*Cp/2	Mach	Re/m	Re_delta_L	Delta_L (mm)	X-station (m)	Re_L	lu/delta_L	delta_P/P
24	6.705E+05	2.90	6.0526E+06	3.8737E+04	6.40E+00	3.71E-01	2.25E+06	0.20	3.51187705

Table 14 Turbulent data - RANS - Ramesh and Tannehill, 2001 – Low Re

Re*Cp/2	Mach	Re/m	Re_delta_L	Delta_L (m)	X-station (m)	Re_L	lu/delta_L	delta_P/P
1.009E+05	2.50	3.3250E+06	2.000E+04	6.02E-03	3.08E-01	1.03E+06	2.1264	0.861
1.032E+05	2.50	3.3250E+06	2.000E+04	6.02E-03	3.08E-01	1.03E+06	2.1762	0.8806
1.368E+05	2.50	3.3250E+06	2.000E+04	6.02E-03	3.08E-01	1.03E+06	2.4254	1.168
1.716E+05	2.50	3.3250E+06	2.000E+04	6.02E-03	3.08E-01	1.03E+06	3.3224	1.465
6.437E+04	4.00	3.3250E+06	2.360E+04	7.10E-03	3.92E-01	1.30E+06	1.764	1.1063
8.717E+04	4.00	3.3250E+06	2.360E+04	7.10E-03	3.92E-01	1.30E+06	2.0181	1.4981
2.531E+04	4.50	3.3250E+06	2.360E+04	7.10E-03	3.97E-01	1.32E+06	1.383	0.5441
6.010E+04	4.50	3.3250E+06	2.360E+04	7.10E-03	3.97E-01	1.32E+06	1.9334	1.2917
8.173E+04	4.50	3.3250E+06	2.360E+04	7.10E-03	3.97E-01	1.32E+06	2.2297	1.7566
2.581E+04	5.00	3.3250E+06	2.580E+04	7.76E-03	4.45E-01	1.48E+06	1.3417	0.611
6.284E+04	5.00	3.3250E+06	2.580E+04	7.76E-03	4.45E-01	1.48E+06	1.961	1.4878
8.576E+04	5.00	3.3250E+06	2.580E+04	7.76E-03	4.45E-01	1.48E+06	2.2319	2.0305
6.107E+04	5.00	4.1560E+06	2.940E+04	7.07E-03	4.14E-01	1.72E+06	1.7217	1.2415
8.583E+04	5.00	4.1560E+06	2.940E+04	7.07E-03	4.14E-01	1.72E+06	2.0181	1.7448

Table 15 Turbulent - RANS - Ramesh and Tannehill (2001) - Mid Re

Re*Cp/2	Mach	Re/m	Re_delta_L	Delta_L (m)	X-station (m)	Re_L	lu/delta_L	delta_P/P
6.292E+05	2.50	3.320E+07	1.277E+05	3.85E-03	2.69E-01	8.91E+06	0.7542	0.6176
1.059E+06	2.50	3.320E+07	1.277E+05	3.85E-03	2.69E-01	8.91E+06	1.0663	1.0397
1.105E+06	2.50	3.320E+07	1.199E+05	3.61E-03	2.49E-01	8.28E+06	1.2217	1.1679
1.447E+06	2.50	3.320E+07	1.361E+05	4.10E-03	2.89E-01	9.60E+06	1.4397	1.3188
4.432E+05	2.96	3.320E+07	1.240E+05	3.73E-03	2.64E-01	8.75E+06	0.5889	0.6210
7.376E+05	2.96	3.320E+07	1.240E+05	3.73E-03	2.64E-01	8.75E+06	0.7762	1.0336
1.003E+06	2.96	3.320E+07	1.311E+05	3.95E-03	2.81E-01	9.34E+06	0.8862	1.3170
1.184E+06	2.96	3.320E+07	1.265E+05	3.81E-03	2.70E-01	8.96E+06	1.3127	1.6210
1.334E+06	2.96	3.320E+07	1.289E+05	3.88E-03	2.76E-01	9.16E+06	1.5198	1.7860
1.427E+06	2.96	3.320E+07	1.265E+05	3.81E-03	2.70E-01	8.96E+06	1.7066	1.9540
1.626E+06	2.96	3.320E+07	1.311E+05	3.95E-03	2.81E-01	9.34E+06	1.8738	2.1350
1.719E+06	2.96	3.320E+07	1.233E+05	3.71E-03	2.62E-01	8.70E+06	2.1815	2.4240
3.441E+05	3.50	3.320E+07	1.311E+05	3.95E-03	2.86E-01	9.50E+06	0.5824	0.6210
7.325E+05	3.50	3.320E+07	1.311E+05	3.95E-03	2.86E-01	9.50E+06	0.8862	1.3220
1.084E+06	3.50	3.320E+07	1.311E+05	3.95E-03	2.86E-01	9.50E+06	1.1901	1.9567
1.183E+06	3.50	3.320E+07	1.311E+05	3.95E-03	2.86E-01	9.50E+06	1.3420	2.1357
1.360E+06	3.50	3.320E+07	1.311E+05	3.95E-03	2.86E-01	9.50E+06	1.6459	2.4540
2.611E+05	4.00	3.320E+07	1.289E+05	3.88E-03	2.85E-01	9.45E+06	0.6697	0.6190
5.558E+05	4.00	3.320E+07	1.289E+05	3.88E-03	2.85E-01	9.45E+06	0.9016	1.3179
6.860E+05	4.00	3.320E+07	1.289E+05	3.88E-03	2.85E-01	9.45E+06	0.9789	1.6267
8.254E+05	4.00	3.320E+07	1.289E+05	3.88E-03	2.85E-01	9.45E+06	1.1334	1.9572
9.544E+05	4.00	3.320E+07	1.265E+05	3.81E-03	2.78E-01	9.24E+06	1.3127	2.3133
1.107E+06	4.00	3.320E+07	1.265E+05	3.81E-03	2.78E-01	9.24E+06	1.5490	2.6839
2.222E+05	4.50	3.320E+07	1.361E+05	4.10E-03	3.07E-01	1.02E+07	0.6344	0.6183
6.029E+05	4.50	3.320E+07	1.289E+05	3.88E-03	2.88E-01	9.56E+06	1.0561	1.7878
8.830E+05	4.50	3.320E+07	1.361E+05	4.10E-03	3.07E-01	1.02E+07	1.2200	2.4577
3.912E+05	2.96	1.603E+07	7.200E+04	4.49E-03	2.90E-01	4.64E+06	1.0236	1.0336

Table 16 Turbulent - RANS - Ramesh and Tannehill (2001) - High Re

Re*Cp/2	Mach	Re/m	Re_delta_L	Delta_L (m)	X-station (m)	Re_L	lu/delta_L	delta_P/P
1.079E+06	2.96	5.0467E+07	1.7180E+05	3.40E-03	2.54E-01	1.28E+07	0.6287	1.0336
1.980E+06	2.96	8.4910E+07	2.8910E+05	3.40E-03	2.77E-01	2.35E+07	0.4699	1.0336
2.700E+06	2.96	1.1074E+08	3.7710E+05	3.41E-03	2.89E-01	3.20E+07	0.4112	1.0336
2.502E+06	2.96	5.0467E+07	3.2680E+05	6.48E-03	5.37E-01	2.71E+07	0.7351	1.1317
1.929E+06	2.96	5.0467E+07	1.9220E+05	3.81E-03	2.89E-01	1.46E+07	0.9189	1.6210
2.905E+06	2.96	7.8022E+07	2.7300E+05	3.50E-03	2.82E-01	2.20E+07	0.7459	1.6210
6.772E+05	2.96	6.7689E+07	2.3690E+05	3.50E-03	2.75E-01	1.86E+07	0.3429	0.4459
8.820E+05	2.96	8.4910E+07	2.9710E+05	3.50E-03	2.86E-01	2.43E+07	0.2937	0.4459

Table 17 Settles et al. (Jan. 1976 – SEC 1) data for Mach 2.95

Pt	Ramp angle (deg)	Lu/delta_o (Fig. 9)	Re*Cp/2	Mach	Re/m	Re_delta_L	Delta_L (in)	X-station (m)	Re_L	delta_P/P
60	10	0.13	3.956E+06	2.95	3.9370E+07	5.2000E+05	5.20E-01	1.18E+00	4.66E+07	1.0343
60	14	0.26	6.196E+06	2.95	3.9370E+07	5.2000E+05	5.20E-01	1.18E+00	4.66E+07	1.6199
60	16	0.48	7.474E+06	2.95	3.9370E+07	5.2000E+05	5.20E-01	1.18E+00	4.66E+07	1.9540
60	18	0.85	8.862E+06	2.95	3.9370E+07	5.2000E+05	5.20E-01	1.18E+00	4.66E+07	2.3169
60	20	1.25	1.037E+07	2.95	3.9370E+07	5.2000E+05	5.20E-01	1.18E+00	4.66E+07	2.7099
100	10	0.10	6.349E+06	2.95	6.2671E+07	7.8000E+05	4.90E-01	1.19E+00	7.48E+07	1.0343
100	14	0.24	9.944E+06	2.95	6.2671E+07	7.8000E+05	4.90E-01	1.19E+00	7.48E+07	1.6199
100	16	0.40	1.199E+07	2.95	6.2671E+07	7.8000E+05	4.90E-01	1.19E+00	7.48E+07	1.9540
100	18	0.72	1.422E+07	2.95	6.2671E+07	7.8000E+05	4.90E-01	1.19E+00	7.48E+07	2.3169
100	20	1.07	1.663E+07	2.95	6.2671E+07	7.8000E+05	4.90E-01	1.19E+00	7.48E+07	2.7099
200	10	0.09	1.319E+07	2.95	1.2415E+08	1.4600E+06	4.63E-01	1.25E+00	1.55E+08	1.0343
200	14	0.18	2.066E+07	2.95	1.2415E+08	1.4600E+06	4.63E-01	1.25E+00	1.55E+08	1.6199
200	16	0.35	2.492E+07	2.95	1.2415E+08	1.4600E+06	4.63E-01	1.25E+00	1.55E+08	1.9540
200	18	0.50	2.955E+07	2.95	1.2415E+08	1.4600E+06	4.63E-01	1.25E+00	1.55E+08	2.3169
200	20	0.90	3.457E+07	2.95	1.2415E+08	1.4600E+06	4.63E-01	1.25E+00	1.55E+08	2.7099
300	10	0.08	1.983E+07	2.95	1.8522E+08	2.0700E+06	4.40E-01	1.26E+00	2.34E+08	1.0343
300	14	0.17	3.105E+07	2.95	1.8522E+08	2.0700E+06	4.40E-01	1.26E+00	2.34E+08	1.6199
300	16	0.27	3.746E+07	2.95	1.8522E+08	2.0700E+06	4.40E-01	1.26E+00	2.34E+08	1.9540
300	18	0.45	4.441E+07	2.95	1.8522E+08	2.0700E+06	4.40E-01	1.26E+00	2.34E+08	2.3169
300	20	0.75	5.194E+07	2.95	1.8522E+08	2.0700E+06	4.40E-01	1.26E+00	2.34E+08	2.7099
500	10	0.08	3.356E+07	2.95	3.0758E+08	3.2500E+06	4.16E-01	1.29E+00	3.95E+08	1.0343
500	14	0.14	5.256E+07	2.95	3.0758E+08	3.2500E+06	4.16E-01	1.29E+00	3.95E+08	1.6199
500	16	0.22	6.340E+07	2.95	3.0758E+08	3.2500E+06	4.16E-01	1.29E+00	3.95E+08	1.9540
500	18	0.38	7.518E+07	2.95	3.0758E+08	3.2500E+06	4.16E-01	1.29E+00	3.95E+08	2.3169
500	20	0.67	8.792E+07	2.95	3.0758E+08	3.2500E+06	4.16E-01	1.29E+00	3.95E+08	2.7099

Table 18 Settles et al. (Jan. 1976 – SEC 2) data for Mach 2.89

Pt	Ramp angle (deg)	Lu/delta_o (Fig. 9)	Re*Cp/2	Mach	Re/m	Re_delta_L	Delta_L (in)	X-station (m)	Re_L	delta_P/P
60	10	0.11	5.445E+08	2.89	3.9370E+07	8.7000E+05	8.70E-01	1.56E+02	6.16E+09	1.0343
60	14	0.25	8.529E+08	2.89	3.9370E+07	8.7000E+05	8.70E-01	1.56E+02	6.16E+09	1.6199
60	16	0.39	1.029E+09	2.89	3.9370E+07	8.7000E+05	8.70E-01	1.56E+02	6.16E+09	1.9540
60	18	0.71	1.220E+09	2.89	3.9370E+07	8.7000E+05	8.70E-01	1.56E+02	6.16E+09	2.3169
60	20	1.11	1.427E+09	2.89	3.9370E+07	8.7000E+05	8.70E-01	1.56E+02	6.16E+09	2.7099
500	18	0.34	1.035E+10	2.89	3.0684E+08	5.4400E+06	6.98E-01	1.70E+02	5.22E+10	2.3169
500	20	0.63	1.211E+10	2.89	3.0684E+08	5.4400E+06	6.98E-01	1.70E+02	5.22E+10	2.7099

Table 19 Settles et al. (Jan. 1976 – SEC 3) data for Mach 2.84

Pt	Ramp angle (deg)	Lu/delta_o (Fig. 9)	Re*Cp/2 (OR) Re/(gamma *M^2) * (Delta P/P)	Re_delta_L	Delta_L (in)	Re_L
60	10	0.13	8.112E+08	1.1900E+06	1.19E+00	8.86E+09
60	14	0.22	1.271E+09	1.1900E+06	1.19E+00	8.86E+09
60	18	0.64	1.817E+09	1.1900E+06	1.19E+00	8.86E+09
60	20	1.15	2.125E+09	1.1900E+06	1.19E+00	8.86E+09
500	10	0.05	7.100E+09	7.6400E+06	9.80E-01	7.75E+10
500	14	0.11	1.112E+10	7.6400E+06	9.80E-01	7.75E+10
500	16	0.19	1.341E+10	7.6400E+06	9.80E-01	7.75E+10
500	18	0.35	1.591E+10	7.6400E+06	9.80E-01	7.75E+10
500	20	0.69	1.860E+10	7.6400E+06	9.80E-01	7.75E+10

Table 20 Settles et al. (Dec. 1976)

Ramp angle (deg)	Re*Cp/2	Mach	Re/m	Re_delta_L	Delta_L (in)	Re_L	lu/delta_L	delta_P/P
24	4.186E+07	2.85	6.2992E+07	1.3280E+06	8.30E-01	1.39E+08	2.00	3.4324763

Table 21 Settles et al., 1979

Ramp angle (deg)	Re*Cp/2	Mach	Re/m	Re_delta_L	Delta_L (cm)	Re_L	lu/delta_L	delta_P/P
24	5.503E+07	2.85	7.3000E+07	1.6790E+06	2.30E+00	1.82E+08	2.00	3.4324763
20	4.153E+07	2.85	7.3000E+07	1.6790E+06	2.30E+00	1.82E+08	1.00	2.59044451
16	3.000E+07	2.85	7.3000E+07	1.6790E+06	2.30E+00	1.82E+08	0.30	1.87125497
8	1.206E+07	2.85	7.3000E+07	1.6790E+06	2.30E+00	1.82E+08	0.15	0.7519938

Table 22 Kuntz et al. - 1987

Ramp angle (deg)	Re*Cp/2	Mach	Re/m	Re_delta_L	Delta_L (mm)	Re_L	lu/delta_L	delta_P/P
8	1.638E+06	2.94	3.7485E+07	3.1000E+05	8.27E+00	2.55E+07	0.15	0.77780101
12	2.755E+06	2.94	3.7485E+07	3.1000E+05	8.27E+00	2.55E+07	0.30	1.30835125
16	4.096E+06	2.94	3.7485E+07	3.1000E+05	8.27E+00	2.55E+07	0.91	1.94562067
20	5.680E+06	2.94	3.7485E+07	3.1000E+05	8.27E+00	2.55E+07	1.81	2.69773571
24	7.531E+06	2.94	3.7485E+07	3.1000E+05	8.27E+00	2.55E+07	3.63	3.57670258

Table 23 Dolling and Or - 1985

Ramp angle (deg)	Re*Cp/2	Mach	Re/m	Re_delta_L	Delta_L (cm)	Re_L	lu/delta_L	delta_P/P
12	5.310E+06	2.90	6.5000E+07	5.3950E+05	8.30E-01	4.86E+07	0.20	1.2873
16	7.888E+06	2.90	6.5000E+07	5.3950E+05	8.30E-01	4.86E+07	0.40	1.9123
20	1.093E+07	2.90	6.5000E+07	5.3950E+05	8.30E-01	4.86E+07	1.00	2.6496
24	1.449E+07	2.90	6.5000E+07	5.3950E+05	8.30E-01	4.86E+07	2.20	3.5119

Table 24 Data from Roshko and Thomke - 1970

Ramp angle (deg)	Lu_Delta_L_o	Re*Cp/2 (OR) Re/(gamma *M^2) * (Delta P/P)	Mach	Re/in	Re_delta_L	Delta_L (in)	Re_L
10	0.252	2.438E+07	2.95	7.5200E+05	3.17E+06	4.21E+00	2.87E+08
19.9	0.54	6.341E+07	2.95	7.5200E+05	3.17E+06	4.21E+00	2.87E+08
21.1	0.739	6.930E+07	2.95	7.5200E+05	3.17E+06	4.21E+00	2.87E+08
23	1.333	7.920E+07	2.95	7.5200E+05	3.17E+06	4.21E+00	2.87E+08
25	2	9.045E+07	2.95	7.5200E+05	3.17E+06	4.21E+00	2.87E+08
14.9	0.262	6.818E+07	3.93	1.2000E+06	5.70E+06	4.75E+00	5.66E+08
22.9	0.4762	1.335E+08	3.93	1.2000E+06	5.70E+06	4.75E+00	5.66E+08
23.4	0.6905	1.382E+08	3.93	1.2000E+06	5.70E+06	4.75E+00	5.66E+08
24.4	1.095	1.481E+08	3.93	1.2000E+06	5.70E+06	4.75E+00	5.66E+08
24.9	1.2143	1.531E+08	3.93	1.2000E+06	5.70E+06	4.75E+00	5.66E+08
26.8	2.11905	1.731E+08	3.93	1.2000E+06	5.70E+06	4.75E+00	5.66E+08
14.9	0.2098	5.702E+07	4.92	9.5900E+05	5.26E+06	5.49E+00	5.30E+08
24	0.3636	1.248E+08	4.92	9.5900E+05	5.26E+06	5.49E+00	5.30E+08
24.9	0.5874	1.329E+08	4.92	9.5900E+05	5.26E+06	5.49E+00	5.30E+08
25.9	0.76923	1.422E+08	4.92	9.5900E+05	5.26E+06	5.49E+00	5.30E+08
27	2.014	1.527E+08	4.92	9.5900E+05	5.26E+06	5.49E+00	5.30E+08

Table 25 Thomke and Roshko (1969) data

Figure from reference	Ramp angle (deg)	Re*Cp/2	Mach	Re/m	Re_delta_L	Delta_L (in)	Re_L	lu/delta_L	delta_P/P
fig. 6	5.16	1.221E+07	1.95	2.2835E+07	1.891E+06	3.26E+00	2.03E+08	0.613	0.3209
fig. 6	9.03	2.331E+07	1.95	2.2835E+07	1.891E+06	3.26E+00	2.03E+08	0.920	0.6127
fig. 6	9.99	2.637E+07	1.95	2.2835E+07	1.891E+06	3.26E+00	2.03E+08	1.043	0.6929
fig. 6	11.08	3.000E+07	1.95	2.2835E+07	1.891E+06	3.26E+00	2.03E+08	1.074	0.7883
fig. 6	12.09	3.353E+07	1.95	2.2835E+07	1.891E+06	3.26E+00	2.03E+08	1.227	0.8811
fig. 6	12.6	3.538E+07	1.95	2.2835E+07	1.891E+06	3.26E+00	2.03E+08	1.227	0.9296
fig. 6	12.94	3.663E+07	1.95	2.2835E+07	1.891E+06	3.26E+00	2.03E+08	1.227	0.9626
fig. 7	8.96	4.186E+07	1.95	4.0236E+07	3.148E+06	3.08E+00	3.67E+08	1.299	0.6069
fig. 7	10.03	4.803E+07	1.95	4.0236E+07	3.148E+06	3.08E+00	3.67E+08	1.299	0.6964
fig. 7	10.97	5.369E+07	1.95	4.0236E+07	3.148E+06	3.08E+00	3.67E+08	1.299	0.7785
fig. 7	12.08	6.070E+07	1.95	4.0236E+07	3.148E+06	3.08E+00	3.67E+08	1.299	0.8801
fig. 7	13	6.680E+07	1.95	4.0236E+07	3.148E+06	3.08E+00	3.67E+08	1.623	0.9685
fig. 8	18.95	4.267E+07	2.95	1.6181E+07	1.874E+06	4.56E+00	2.08E+08	0.658	2.4998
fig. 8	19.92	4.598E+07	2.95	1.6181E+07	1.874E+06	4.56E+00	2.08E+08	0.658	2.6936
fig. 8	21.03	4.992E+07	2.95	1.6181E+07	1.874E+06	4.56E+00	2.08E+08	0.877	2.9244
fig. 8	21.88	5.305E+07	2.95	1.6181E+07	1.874E+06	4.56E+00	2.08E+08	1.096	3.1080
fig. 9	10	3.255E+07	2.95	2.9606E+07	3.166E+06	4.21E+00	3.83E+08	0.238	1.0343
fig. 9	14.88	5.549E+07	2.95	2.9606E+07	3.166E+06	4.21E+00	3.83E+08	0.238	1.7634
fig. 9	16.84	6.617E+07	2.95	2.9606E+07	3.166E+06	4.21E+00	3.83E+08	0.356	2.1029
fig. 9	19.92	8.476E+07	2.95	2.9606E+07	3.166E+06	4.21E+00	3.83E+08	0.713	2.6936
fig. 9	20.46	8.826E+07	2.95	2.9606E+07	3.166E+06	4.21E+00	3.83E+08	0.736	2.8047
fig. 9	21.09	9.243E+07	2.95	2.9606E+07	3.166E+06	4.21E+00	3.83E+08	0.772	2.9372
fig. 9	21.52	9.534E+07	2.95	2.9606E+07	3.166E+06	4.21E+00	3.83E+08	0.950	3.0295
fig. 9	23.04	1.060E+08	2.95	2.9606E+07	3.166E+06	4.21E+00	3.83E+08	1.425	3.3685
fig. 9	25	1.207E+08	2.95	2.9606E+07	3.166E+06	4.21E+00	3.83E+08	2.138	3.8365
fig. 10	20.02	1.332E+08	2.95	5.9409E+07	4.633E+06	3.07E+00	5.98E+08	0.651	2.7140
fig. 10	21.45	1.479E+08	2.95	5.9409E+07	4.633E+06	3.07E+00	5.98E+08	0.977	3.0144
fig. 10	21.92	1.529E+08	2.95	5.9409E+07	4.633E+06	3.07E+00	5.98E+08	1.270	3.1168
fig. 10	21.96	1.534E+08	2.95	5.9409E+07	4.633E+06	3.07E+00	5.98E+08	1.303	3.1256
fig. 10	24	1.763E+08	2.95	5.9409E+07	4.633E+06	3.07E+00	5.98E+08	2.248	3.5931
fig. 11	17.87	4.483E+07	3.93	1.7441E+07	2.374E+06	5.36E+00	2.82E+08	0.466	3.4337
fig. 11	18.85	4.872E+07	3.93	1.7441E+07	2.374E+06	5.36E+00	2.82E+08	0.466	3.7323
fig. 11	19.88	5.299E+07	3.93	1.7441E+07	2.374E+06	5.36E+00	2.82E+08	0.541	4.0591
fig. 11	21.98	6.224E+07	3.93	1.7441E+07	2.374E+06	5.36E+00	2.82E+08	0.550	4.7672
fig. 11	22.47	6.450E+07	3.93	1.7441E+07	2.374E+06	5.36E+00	2.82E+08	0.550	4.9405
fig. 11	23.44	6.909E+07	3.93	1.7441E+07	2.374E+06	5.36E+00	2.82E+08	0.933	5.2926
fig. 11	23.97	7.167E+07	3.93	1.7441E+07	2.374E+06	5.36E+00	2.82E+08	1.119	5.4901
fig. 11	26.82	8.636E+07	3.93	1.7441E+07	2.374E+06	5.36E+00	2.82E+08	2.146	6.6154
fig. 12	14.99	5.752E+07	3.93	2.8898E+07	3.699E+06	5.04E+00	4.74E+08	0.198	2.6265
fig. 12	20.03	8.996E+07	3.93	2.8898E+07	3.699E+06	5.04E+00	4.74E+08	0.417	4.1078
fig. 12	21.05	9.738E+07	3.93	2.8898E+07	3.699E+06	5.04E+00	4.74E+08	0.522	4.4467
fig. 12	21.51	1.008E+08	3.93	2.8898E+07	3.699E+06	5.04E+00	4.74E+08	0.552	4.6038
fig. 12	22.45	1.080E+08	3.93	2.8898E+07	3.699E+06	5.04E+00	4.74E+08	0.637	4.9333
fig. 12	23.04	1.127E+08	3.93	2.8898E+07	3.699E+06	5.04E+00	4.74E+08	0.661	5.1459
fig. 12	25.01	1.289E+08	3.93	2.8898E+07	3.699E+06	5.04E+00	4.74E+08	1.411	5.8882
fig. 13	14.9	9.439E+07	3.93	4.7244E+07	5.700E+06	4.75E+00	7.84E+08	0.438	2.6030
fig. 13	15.06	9.591E+07	3.93	4.7244E+07	5.700E+06	4.75E+00	7.84E+08	0.438	2.6449
fig. 13	18.55	1.320E+08	3.93	4.7244E+07	5.700E+06	4.75E+00	7.84E+08	0.404	3.6396
fig. 13	22.9	1.848E+08	3.93	4.7244E+07	5.700E+06	4.75E+00	7.84E+08	0.632	5.0951
fig. 13	22.94	1.853E+08	3.93	4.7244E+07	5.700E+06	4.75E+00	7.84E+08	0.632	5.1096
fig. 13	23.42	1.917E+08	3.93	4.7244E+07	5.700E+06	4.75E+00	7.84E+08	0.842	5.2852
fig. 13	24.42	2.053E+08	3.93	4.7244E+07	5.700E+06	4.75E+00	7.84E+08	1.211	5.6606
fig. 13	24.92	2.123E+08	3.93	4.7244E+07	5.700E+06	4.75E+00	7.84E+08	1.263	5.8532
fig. 13	26.83	2.400E+08	3.93	4.7244E+07	5.700E+06	4.75E+00	7.84E+08	2.105	6.6195
fig. 13	26.94	2.417E+08	3.93	4.7244E+07	5.700E+06	4.75E+00	7.84E+08	2.211	6.6651
fig. 14	23	2.714E+08	3.93	6.8622E+07	7.878E+06	4.52E+00	1.14E+09	0.466	5.1313
fig. 14	23.94	2.898E+08	3.93	6.8622E+07	7.878E+06	4.52E+00	1.14E+09	0.675	5.4788
fig. 14	25.05	3.123E+08	3.93	6.8622E+07	7.878E+06	4.52E+00	1.14E+09	1.164	5.9038
fig. 14	26.91	3.519E+08	3.93	6.8622E+07	7.878E+06	4.52E+00	1.14E+09	2.073	6.6527
fig. 15	19.97	7.211E+07	4.92	2.2047E+07	3.254E+06	5.81E+00	4.17E+08	0.229	5.8627
fig. 15	21.08	7.892E+07	4.92	2.2047E+07	3.254E+06	5.81E+00	4.17E+08	0.344	6.4159
fig. 15	21.45	8.125E+07	4.92	2.2047E+07	3.254E+06	5.81E+00	4.17E+08	0.361	6.6056
fig. 15	22.98	9.125E+07	4.92	2.2047E+07	3.254E+06	5.81E+00	4.17E+08	0.471	7.4187
fig. 15	24.93	1.048E+08	4.92	2.2047E+07	3.254E+06	5.81E+00	4.17E+08	1.087	8.5205
fig. 16	14.86	7.834E+07	4.92	3.7756E+07	5.265E+06	5.49E+00	7.31E+08	0.182	3.6324
fig. 16	24.02	1.725E+08	4.92	3.7756E+07	5.265E+06	5.49E+00	7.31E+08	0.364	7.9972
fig. 16	24.93	1.838E+08	4.92	3.7756E+07	5.265E+06	5.49E+00	7.31E+08	0.863	8.5205
fig. 16	25.88	1.959E+08	4.92	3.7756E+07	5.265E+06	5.49E+00	7.31E+08	0.911	9.0837
fig. 16	26.96	2.102E+08	4.92	3.7756E+07	5.265E+06	5.49E+00	7.31E+08	2.013	9.7450

Table 26 Data from Law for Mach 2.96 (1974)

Ramp angle (deg)	Lu_Delta_L_o	Re*Cp/2	Mach	Re/m	Re_delta_L	Delta_L (in)	Re_L	delta_P/P	Cp/2
15	0.941176471	2.612E+06	2.96	3.4738E+07	1.50E+05	1.70E-01	1.09E+07	2.93128919	2.390E-01
17	1.205882353	2.806E+06	2.96	3.4738E+07	1.50E+05	1.70E-01	1.09E+07	3.14869692	2.567E-01
19	1.394117647	3.007E+06	2.96	3.4738E+07	1.50E+05	1.70E-01	1.09E+07	3.37463164	2.751E-01
21	2.111764706	3.217E+06	2.96	3.4738E+07	1.50E+05	1.70E-01	1.09E+07	3.60953929	2.943E-01
23	2.714705882	3.434E+06	2.96	3.4738E+07	1.50E+05	1.70E-01	1.09E+07	3.85401777	3.142E-01
25	3.770588235	3.662E+06	2.96	3.4738E+07	1.50E+05	1.70E-01	1.09E+07	4.10888779	3.350E-01

Table 27 - Roshko and Thomke Data (1970) – does not follow Cp^2 trend

Ramp angle (deg)	Lu_Delta_L_o	Re*Cp/2	Mach	Re/m	Re_delta_L	Delta_L (in)	Re_L	delta_P/P	Cp/2
14.9	0.262	9.439E+07	3.93	4.7244E+07	5.70E+06	4.75E+00	7.84E+08	2.6030	1.204E-01
22.9	0.4762	1.848E+08	3.93	4.7244E+07	5.70E+06	4.75E+00	7.84E+08	5.0951	2.356E-01
23.4	0.6905	1.914E+08	3.93	4.7244E+07	5.70E+06	4.75E+00	7.84E+08	5.2778	2.441E-01
24.4	1.095	2.050E+08	3.93	4.7244E+07	5.70E+06	4.75E+00	7.84E+08	5.6530	2.614E-01
24.9	1.2143	2.120E+08	3.93	4.7244E+07	5.70E+06	4.75E+00	7.84E+08	5.8454	2.703E-01
26.8	2.11905	2.396E+08	3.93	4.7244E+07	5.70E+06	4.75E+00	7.84E+08	6.6071	3.056E-01
14.9	0.2098	7.859E+07	4.92	3.7721E+07	5.26E+06	5.49E+00	7.30E+08	3.6478	1.076E-01
24	0.3636	1.720E+08	4.92	3.7721E+07	5.26E+06	5.49E+00	7.30E+08	7.9859	2.356E-01
24.9	0.5874	1.832E+08	4.92	3.7721E+07	5.26E+06	5.49E+00	7.30E+08	8.5030	2.509E-01
25.9	0.76923	1.960E+08	4.92	3.7721E+07	5.26E+06	5.49E+00	7.30E+08	9.0957	2.684E-01
27	2.014	2.105E+08	4.92	3.7721E+07	5.26E+06	5.49E+00	7.30E+08	9.7699	2.883E-01

Table 28 - Thomke & Roshko (1969) data - does not follow Cp^2 trend

Figure from reference	Ramp angle (deg)	Re*Cp/2	Mach	Re/m	Re_delta_L	Delta_L (in)	Re_L	lu/delta_L	delta_P/P
fig. 6	5.16	1.221E+07	1.95	2.2835E+07	1.891E+06	3.26E+00	2.03E+08	0.613	0.3209
fig. 6	9.03	2.331E+07	1.95	2.2835E+07	1.891E+06	3.26E+00	2.03E+08	0.920	0.6127
fig. 6	9.99	2.637E+07	1.95	2.2835E+07	1.891E+06	3.26E+00	2.03E+08	1.043	0.6929
fig. 6	11.08	3.000E+07	1.95	2.2835E+07	1.891E+06	3.26E+00	2.03E+08	1.074	0.7883
fig. 6	12.09	3.353E+07	1.95	2.2835E+07	1.891E+06	3.26E+00	2.03E+08	1.227	0.8811
fig. 6	12.6	3.538E+07	1.95	2.2835E+07	1.891E+06	3.26E+00	2.03E+08	1.227	0.9296
fig. 6	12.94	3.663E+07	1.95	2.2835E+07	1.891E+06	3.26E+00	2.03E+08	1.227	0.9626
fig. 13	14.9	9.439E+07	3.93	4.7244E+07	5.700E+06	4.75E+00	7.84E+08	0.438	2.6030
fig. 13	22.9	1.848E+08	3.93	4.7244E+07	5.700E+06	4.75E+00	7.84E+08	0.632	5.0951
fig. 13	23.42	1.917E+08	3.93	4.7244E+07	5.700E+06	4.75E+00	7.84E+08	0.842	5.2852
fig. 13	24.42	2.053E+08	3.93	4.7244E+07	5.700E+06	4.75E+00	7.84E+08	1.211	5.6606
fig. 13	26.83	2.400E+08	3.93	4.7244E+07	5.700E+06	4.75E+00	7.84E+08	2.105	6.6195
fig. 14	23	2.714E+08	3.93	6.8622E+07	7.878E+06	4.52E+00	1.14E+09	0.466	5.1313
fig. 14	23.94	2.898E+08	3.93	6.8622E+07	7.878E+06	4.52E+00	1.14E+09	0.675	5.4788
fig. 14	25.05	3.123E+08	3.93	6.8622E+07	7.878E+06	4.52E+00	1.14E+09	1.164	5.9038
fig. 14	26.91	3.519E+08	3.93	6.8622E+07	7.878E+06	4.52E+00	1.14E+09	2.073	6.6527

Table 29 - Data from Thomas et al. (1994)

Ramp angle (deg)	Re*Cp/2	Mach	Re/m	Re_delta_L	Delta_L (mm)	Re_L	lu/delta_L	delta_P/P
6	1.384E+06	1.50	1.2500E+07	1.7875E+05	1.43E+01	1.27E+07	1.43	0.3432835
9	2.306E+06	1.50	1.2500E+07	1.7875E+05	1.43E+01	1.27E+07	2.00	0.57183694
12	3.898E+06	1.50	1.2500E+07	1.7875E+05	1.43E+01	1.27E+07	2.50	0.96677935

Table 30 Data from Selig et al. (1989)

Ramp angle (deg)	Re*Cp/2	Mach	Re/m	Re_delta_L	Delta_L (cm)	Re_L	lu/delta_L	delta_P/P
24	5.557E+07	2.84	6.5000E+07	1.6900E+06	2.60E+00	1.84E+08	1.73	3.41681924

Table 31 Erengil and Dolling (May 1991)

Ramp angle (deg)	Re*Cp/2	Mach	Re/m	Re_delta_L	Delta_L (cm)	Re_L	lu/delta_L	delta_P/P
28	2.736E+07	4.95	4.9600E+07	8.6800E+05	1.75E+00	8.93E+07	2.75	10.5143711

Table 32 Huo (2003)

Ramp angle (deg)	Re*Cp/2	Mach	Re/m	Re_delta_L	Delta_L (mm)	Re_L	lu/delta_L	delta_P/P
20	1.129E+07	2.00	3.3000E+07	4.1184E+05	1.25E+01	3.43E+07	2.70	1.8428627

Table 33 Ganapathisubramani et al. (2007)

Ramp angle (deg)	Re*Cp/2	Mach	Re/m	Re_delta_L	Delta_L (mm)	Re_L	lu/delta_L	delta_P/P
20	1.369E+07	2.00	3.8889E+07	4.8611E+05	1.25E+01	4.16E+07	1.25	1.8428627

Table 34 Ringuette et al. (2009) (experiment)

Ramp angle (deg)	Re*Cp/2	Mach	Re/m	Re_delta_L	Delta_L (mm)	Re_L	lu/delta_L	delta_P/P
24	6.435E+05	2.90	5.5814E+06	3.7395E+04	6.70E+00	2.16E+06	3.60	3.51187705

Acknowledgments

The author appreciates the many people that have helped with this effort. The experimental team of the Mach 6 High Reynolds Number Test Facility (Mr. Jim Hayes, Dr. Frank Semmelmayer, Mr. Ben Hagen, Ms. Servane Altman) for their outstanding support of the test. To Capt. Sam Nyameke, and Capt. Evan Oren for their support in executing the tests and analysis of data. Dr. Roger Kimmel for his help during the test campaign and design of the model. Dr. Matt Borg, Dr. Cam Carter, Mr. David Adamczak and Mr. Kevin King for help in diagnostics for the model. Dr. Ryan Durscher for many CFD solutions to help in the design of the model. Mr. Ryan Merritt for development of the models. A special thanks to Dr. Matt Borg for reviewing an earlier version of this abstract and providing very helpful guidance.

References

[1] Ferri, A., "Experimental Results with Airfoils Tested in the High Speed Tunnel at Guidonia," NACA TM 946, 1940.
[2] Decker, R. K., Miller, J.H., "Reduced Domain Method Applied to a Mach 6.9 Circular Arc Airfoil with a Trailing Edge Flap", AIAA Paper 2019-0278, Jan. 2019.
[3] Lighthill, M.J., "On boundary layers and upstream influence. I. A comparison between subsonic and supersonic flows, Proceedings of the Royal Society of London Series A – Mathematical and Physical Sciences, Vol. 217, Issue 1130, pp. 344-357, 1953.
[4] Chapman, D.R., Kuehn, D.M., and Larson, H.K., "Investigation of Separated Flows in Supersonic and Subsonic Streams with Emphasis on the Effect of Transition," NACA Technical Note 3869, March 1957.
[5] Delery, J., and Marvin, J.G., "Shock-Wave Boundary-Layer Interactions," *AGARDograph* AG-280, Feb. 1986.
[6] Dolling, D.S., "Fifty Years of Shock-Wave/Boundary-Layer Interaction Research: What Next?", AIAA Journal, Vol. 39, No. 8, pp. 1517-1531, August 2001.
[7] Gaitonde, D.V., "Progress in shock wave/boundary layer interactions", Progress in Aerospace Sciences, Vol. 72, pp. 80-99, 2015 – published by Elsevier.
[8] Lighthill, M.J., "On Boundary Layers and Upstream Influence II. Supersonic Flows Without Separation," Proceedings of the Royal Society A, Vol. 217, 1953, pp. 478-507.
[9] Lighthill, M.J., "Upstream Influence in Boundary Layers 45 Years Ago," Philosophical Transactions of the Royal Society A – Mathematical, Physical and Engineering Sciences, Vol. 358, Issue 1777, pp. 3047-3061, 2000 – from EUROMECH 384 Colloquium on Steady and Unsteady Separated Flows, Dec. 15, 2000.
[10] Needham, D.A., and Stollery, J.L., "Boundary Layer Separation in Hypersonic Flow", AIAA Paper 66-455, June 1966.
[11] Roberts, M.L., "Transitional Flow Separation Upstream of a Compression Corner", Journal of Spacecraft, Vol. 7, No. 9, Sept. 1970, pp. 1113-1117.
[12] Gray, J.D., and Rhudy, R.W., "Effects of Blunting and Cooling on Separation of Laminar Supersonic Flow," AIAA Journal, Vol. 11, No. 9, Sept. 1973, pp. 1296-1301.

[13] Holden, M., and Chadwick, K., "Studies of Laminar, Transitional and Turbulent Hypersonic Flows Over Curved Compression Surfaces", AIAA Paper 95-0093, Jan. 1995.
[14] Knight, D., and Mortazavi, M., "Hypersonic Shock Wave Transitional Boundary Layer Interactions – A Review", AIAA Paper 2017-3124, June 2017.
[15] Balakumar, P., Zhao, H., and Atkins, H., "Stability of Hypersonic Boundary-Layers Over a Compression Corner," AIAA Paper 2002-2848, June 2002.
[16] Whalen, T., Kennedy, R., Laurence, S., Sullivan, B., Bodony, D., and Buck, G., "Unsteady Surface and Flowfield Measurements in Ramp-Induced Turbulent and Transitional Shock-Wave Boundary-Layer Interactions at Mach 6", AIAA Paper 2019-1127, Jan. 2019.
[17] Threadgill, J.A.S., Little, J.C., Wernz, S.H., "Transitional Shock Boundary Layer Interactions on a Compression Ramp at Mach 4," AIAA Journal, Vol. 59, No. 12, Dec. 2021, pp. 4824-4841.
[18] Cao, S., Hao, J., Klioutchnikov, I., Wen, C-Y, Olivier, H., and Heufer, K.A., "Transition to Turbulence in Hypersonic Flow Over a Compression Ramp Due to Intrinsic Instability", Journal of Fluid Mechanics, Vol. 941, A8, pp. 941 A8-1 – A8-26 (online).
[19] Frew, D., Galassi, L., Stava, D., and Azevedo, D. "Influence of Boundary-Layer Transition on Measured Incipient Separation Angles", Journal of Propulsion and Power, Vol. 11, No. 5, Sept.-Oct. 1995, pp. 938-942.
[20] Povitsky, A., Miller, J.H., Barua, H., "Shock Wave Interaction with Boundary Layer at Ramp Surface", AIAA Paper 2021-1311, Jan. 2021.
[21] Kimmel, R., personal communication, June 2014.
[22] Schneider, S.P., "Effects of Roughness on Hypersonic Boundary-Layer Transition," Journal of Spacecraft and Rockets, Vol. 45, No. 2, March-April 2008, pp. 193-209.
[23] Chism, J.R., Gragston, M., Hagen, B., Leicht, J., and Riley, Z., "Freestream Characterization of the AFRL Mach 6 High Reynolds Facility using Laser Induced Schliere Anemometry with Collinear Light Entry", AIAA Paper 2022-3473, June 2022.
[24] Spalding, D.B., and Chi,, S.W., "The Drag of A Compressible Turbulent Boundary Layer on a Smooth Flat Plate With and Without Heat Transfer", Journal of Fluid Mechanics, Vol. 18, Pt. 1, pp. 117-143, Jan. 1964.
[25] Holden, M.S., "Shock Wave-Turbulent Boundary Layer Interaction in Hypersonic Flow", AIAA Paper 77-45, Jan. 1977.
[26] Eckert, E.R.G., "Engineering Relations for Friction and Heat Transfer to Surfaces in High Velocity Flow", Journal of Aeronautical Sciences, Vol. 23, No. 8, pp. 585-587, 1956.
[27] Schmit, R.F., Semmelmayer, F., Haverkamp, M., and Grove, J.E., "Fourier Analysis of High Speed Shadowgraph Images Around a Mach 1.5 Cavity Flow Field", AIAA Paper 2011-3961, June 2011.
[28] Roshko, A. and Thomke, G.J., "Flare-Induced Interaction Lengths in Supersonic, Turbulent Boundary Layers," AIAA Journal, Vol. 14, No. 7, July 1976, pp. 873-879.
[29] Miller, J.H., Tannehill, J.C., and Lawrence, S.L., "Parabolized Navier-Stokes Algorithm for Solving Supersonic Flows with Upstream Influences," *AIAA Journal*, Vol. 38, No. 10, Oct. 2000, pp. 1837-1845.
[30] Davis, S.K., Ward, T., Shellabarger, E., and Miller, J.H., "Laminar Hypersonic Flow Over Compression Ramp With Sharp Leading Edge: Separation and Upstream Influence", Presentation at 74th Annual Meeting of the American Physical Society, Fluid Dynamics Division, Nov. 2021.
[31] Ward, T., Shellaberger, E., and Davis, S.K., "Matched Asymptotic Shock-Layer Analysis of the Interaction Between a Planar Viscous-Hypersonic Boundary Layer and a Thin Inviscid Layer", Theoretical Computational Fluid Dynamics, https://doi.org/10.1007/s00162-022-00611-4, Vol. 36, pp. 545-573, May 2022
[32] Stewartson, K. and Williams, P.G., "Self-Induced Separation," Proceedings of the Royal Society A, Vol. 312, 1969, pp. 181-206.
[33] Schlichting, H., "Boundary Layer Theory", seventh edition, 1979, pp. 206-208, McGraw-Hill Book Company.
[34] Pohlhausen, K.: Zur näherungsweisen Integration der Differentialgleichung der laminaren Reibungsschicht. ZAAM Vol. 1, pp. 252-268, 1921.
[35] Miller, J.H., "Elliptic Length Scales in Laminar, Two-Dimensional Supersonic Flows," AFRL-RQ-WP-TP-2015-0109, June 2015.
[36] Tannehill, J.C., Anderson, D.A., and Pletcher, R.H., Computational Fluid Mechanics and Heat Transfer, 2nd Edition, Taylor and Francis, Washington, D.C., 1997.
[37] Karamcheti, K. *Principles of Ideal-Fluid Aerodynamics*, John Wiley and Sons, Inc., New York, 1966. Pp. 16-17.
[38] Ramesh, M.D., and Tannehill, J.C., "Correlations to Predict the Streamwise Influence Regions of 2-D Supersonic Turbulent Flows," AIAA Paper 2001-0884, Jan. 2001.
[39] Settles, G.S and Bogdonoff, S.M., "Scaling of Two- and Three-Dimensional Shock/Turbulent Boundary-Layer Interactions at Compression Corners," AIAA Journal, Vol. 20, No. 6, June 1982, pp. 782-789.

[40] Wei, T., “Analysis of Shock Wave Boundary Layer Interaction”, Final Report, Summer Faculty Fellowship Program, July 2022.
[41] Wei, T., Livescu, D., and Liu, X., “Scaling Patch Analysis of Planar Turbulent Wake”, Physics of Fluids, Vol. 34, no. doi: 10.1063/5.0097588, pp. 065116, 1-7, 2022
[42] Fife, P., Wei, T., Klewicki, J., and McMurtry, P., “Stress Gradient Balance Layers and Scale Hierarchies in Wall-Bounded Turbulent Flows”, Journal of Fluid Mechanics, Vol. 532, pp. 165-189, 2005.
[43] Incropera, F.P., DeWitt, D.P., “Fundamentals of Heat and Mass Transfer,” John Wiley & Sons, Inc., 1990, pp. 472-474.
[44] Simeonides, G., Haase, W., and Manna, M., “Experimental, Analytical, and Computational Methods Applied to Hypersonic Compression Ramp Flows”, AIAA Journal, Vol. 32, No. 2, Feb. 1994, pp. 301-310.
[45] Lewis, J.E., Kubota, T., and Lees, L., ”Experimental Investigation of Supersonic Laminar, Two-Dimensional Boundary-Layer Separation in a Compression Corner with and without Cooling”, AIAA Journal, Vol. 6, No. 1, Jan. 1968, pp. 7-14.
[46] Ringuette, M.J., Bookey, P., Wyckham, Ch., and Smits, A.J., “Experimental Study of a Mach 3 Compression Ramp Interaction at Re-theta = 2400”, AIAA Journal Vol. 47, No. 2, Feb. 2009, pp. 373-385.
[47] Thomas, F.O., Putnam, C.M., and Chu, H.C., “On the Mechanism of Unsteady Shock Oscillation in Shock Wave/Turbulent Boundary Layer Interactions”, Experiments in Fluids, Vol. 18, pp. 69-81, 1994.
[48] Law, C.H., “Supersonic, Turbulent Boundary-Layer Separation,” AIAA Journal, Vol. 12, No. 6, June 1974, pp. 794-797.
[49] Roshko, A. and Thomke, G.J., “Supersonic, Turbulent Boundary-Layer Interaction with a Compression Corner at Very High Reynolds Number,” Proceedings of the 1969 Symposium, Viscous Interaction Phenomena in Supersonic and Hypersonic Flow, 1970, University of Dayton Press, Dayton, Ohio, pp. 109-138.
[50] Thomke, G.J., and Roshko, A., “Incipient Separation of a Turbulent Boundary Layer at High Reynolds Number in Two-Dimensional Supersonic Flow Over a Compression Corner”, NASA Final Report, NASA CR-73308, Jan. 1969.
[51] Selig, M.S., Andreopoulos, J., Muck, K.C., Dussauge, J.P., Smits, A.J., “Turbulence Structure in a Shock Wave/Turbulent Boundary-Layer Interaction”, AIAA Journal, Vol. 27, No. 7, July 1989, pp. 862-869.
[52] Erengil, M.E., and Dolling, D.S., “Unsteady Wave Structure near Separation in a Mach 5 Compression Ramp Interaction”, AIAA Journal, Vol. 29, No. 5,1991, pp. 728-735.
[53] Hou, Y., “Particle Image Velocimetry Study of Shock Induced Turbulent Boundary Layer Separation”, Ph.D. Dissertation, University of Texas at Austin, Dec. 2003.
[54] Ganapathisubramani, B., Clemens, N.T., and Dolling D.S., “Effects of Upstream Coherent Structures on Low-Frequency Motion of Shock-Induced Turbulent Separation”, AIAA Paper 2007-1141, Jan. 2007.
[55] Wu, M., and Martin, M.P., “Analysis of Shock Motion in Shockwave and Turbulent Boundary Layer Interaction Using Direct Numerical Simulation Data”, Journal of Fluid Mechanics, Vol. 594, pp. 71-83, 2008.
[56] Souverein, L.J., Bakker, P.G., and Dupont, P., “A Scaling Analysis for Turbulent Shock-Wave/Boundary-Layer Interactions”, Journal of Fluid Mechanics, Vol. 714, pp. 505-535, 2013.
[57] Running, C.L., Juliano, T.J., Jewell, J.S., Borg, M.P., and Kimmel, R.L., “Hypersonic Shock-Wave/Boundary-Layer Interactions on a Cone/Flare”, Experimental Thermal and Fluid Science, Vol. 109 (2019), 109911 (Online).
[58] Ames Research Staff, “Equations, Tables, and Charts for Compressible Flow”, NACA Report 1135, 1953.
[59] Settles, G.S., Bogdonoff, S.M., and Vas, I.E., “Incipient Separation of a Supersonic Turbulent Boundary Layer at High Reynolds Numbers, “ AIAA Journal, Vol. 14, No. 1, Jan. 1976, pp. 50-56.
[60] Settles, G.S., Fitzpatrick, T.J., Bogdonoff, S.M., “Detailed Study of Attached and Separated Compression Corner Flowfields in High Reynolds Number Supersonic Flow,” AIAA Journal, Vol. 17, No. 6, June 1979, pp. 579-585.
[61] Settles, G.S., Vas, I.E., and Bogdonoff, S.M., “Details of a Shock-Separated Turbulent Boundary Layer at a Compression Corner”, AIAA Journal, Vol. 14, No. 12, Dec. 1976, pp. 1709-1715.